Cerebral dopamine neurotrophic factor–deficiency leads to degeneration of enteric neurons and altered brain dopamine neuronal function in mice

Maria Lindahl[a,*], **Alcmène Chalazonitis**[b], **Erik Palm**[a], **Emmi Pakarinen**[a], **Tatiana Danilova**[a], **Tuan D. Pham**[b], **Wanda Setlik**[b], **Meenakshi Rao**[b,1], **Vootele Võikar**[c], **Jatta Huotari**[a], **Jaakko Kopra**[d], **Jaan-Olle Andressoo**[a,2], **Petteri T. Piepponen**[d], **Mikko Airavaara**[a], **Anne Panhelainen**[a], **Michael D. Gershon**[b], **Mart Saarma**[a]

[a]Institute of Biotechnology, HiLIFE Unit, Viikinkaari 5D, FI-00014, University of Helsinki, Finland

[b]Department of Pathology & Cell Biology, Columbia University, NY, New York, USA

[c]Neuroscience Center/Laboratory Animal Center, Mustialankatu 1, FI-00014, University of Helsinki, Finland

[d]Division of Pharmacology and Pharmacotherapy, Faculty of Pharmacy, Viikinkaari 5E, FI-00014, University of Helsinki, Finland

Abstract

Cerebral dopamine neurotrophic factor (CDNF) is neuroprotective for nigrostriatal dopamine neurons and restores dopaminergic function in animal models of Parkinson's disease (PD). To understand the role of CDNF in mammals, we generated CDNF knockout mice (*Cdnf$^{-/-}$*), which are viable, fertile, and have a normal life-span. Surprisingly, an age-dependent loss of enteric neurons occurs selectively in the submucosal but not in the myenteric plexus. This neuronal loss is a consequence not of increased apoptosis but of neurodegeneration and autophagy. Quantitatively, the neurodegeneration and autophagy found in the submucosal plexus in duodenum, ileum and colon of the *Cdnf$^{-/-}$* mouse are much greater than in those of *Cdnf$^{+/+}$* mice. The selective vulnerability of submucosal neurons to the absence of CDNF is reminiscent of the tendency of pathological abnormalities to occur in the submucosal plexus in biopsies of patients with PD. In contrast, the number of substantia nigra dopamine neurons and dopamine and its metabolite concentrations in the striatum are unaltered in *Cdnf$^{-/-}$* mice; however, there is an age-dependent deficit in the function of the dopamine system in *Cdnf$^{-/-}$* male mice analyzed. This is observed as D-amphetamine-induced hyperactivity, aberrant dopamine transporter function, and

---

*Corresponding author. maria.lindahl@helsinki.fi (M. Lindahl).
[1]Present address: Division of Gastroenterology, Boston Children's Hospital, Harvard Medical School, Boston, Massachusetts, USA.
[2]Present address: Faculty of Medicine & Helsinki Institute of Life Science, University of Helsinki, P.O. Box 63, 00014 Helsinki, Finland & Division of Neurogeriatrics, Department of Neurobiology, Care Sciences and Society, Karolinska Institutet SE-171 77, Sweden.

as increased D-amphetamine-induced dopamine release demonstrating that dopaminergic axon terminal function in the striatum of the *Cdnf*$^{-/-}$ mouse brain is altered. The deficiencies of *Cdnf*$^{-/-}$ mice, therefore, are reminiscent of those seen in early stages of Parkinson's disease.

Keywords

Cerebral dopamine neurotrophic factor (CDNF); Knockout mouse; Enteric nervous system; Midbrain; Dopaminergic; Dopamine transporter; Neurodegeneration; Autophagy; Parkinson's disease

1. Introduction

Parkinson's disease (PD) is a neurodegenerative disorder characterized by progressive degeneration of dopamine neurons in the substantia nigra pars compacta (SNpc), dramatic decreases in brain dopamine (DA) concentrations, and deficits in motor behavior. PD patients also suffer from dysfunctional gastrointestinal (GI) motility, especially constipation, which frequently occurs before the movement disorder (Pfeiffer, 2003). The exact reason for the GI motility dysfunction in PD is not known; however, deficiencies of enteric dopaminergic and non-dopaminergic neurons have been reported in PD patients (Braak et al., 2006; Chalazonitis and Rao, 2018; Kupsky et al., 1987; Lebouvier et al., 2010; Rao and Gershon, 2016; Singaram et al., 1995).

We and others have shown that CDNF protects midbrain dopamine neurons and restores dopaminergic function in neurotoxin-induced animal models of PD (Airavaara et al., 2012; Garea-Rodriguez et al., 2016; Lindholm et al., 2007; Ren et al., 2013; Voutilainen et al., 2011). Although genome-wide association studies for PD have not identified mutations in the *CDNF* gene, a study of early-onset PD patients identified a single nucleotide polymorphism in the intron between exon 1 and 2 of *CDNF* (Choi et al., 2011).

CDNF and a related protein, mesencephalic astrocyte-derived neurotrophic factor (MANF) (Apostolou et al., 2008; Lindholm et al., 2008; Lindholm et al., 2007; Mizobuchi et al., 2007; Petrova et al., 2003; Voutilainen et al., 2009), form a novel family of cytoprotective factors with two distinct domains, an N-terminal, possibly lipid and membrane interacting domain, and a C-terminal domain containing a non-canonical ER-retention sequence and a conserved CXXC sequence. In fact, MANF, but not CDNF, has been found to bind to lipid sulfatides present on the outer leaflets of plasma membranes, which promotes cellular uptake of MANF and cytoprotection from hypoxia-induced cell death (Bai et al., 2018). CDNF transcripts and protein are expressed, not only in SNpc neurons, but also in several additional areas of the adult mouse and human brain, as well as in multiple peripheral tissues (Lindholm et al., 2007). CDNF and MANF proteins are located mainly in the ER lumen and MANF is secreted upon ER calcium depletion (Apostolou et al., 2008; Glembotski et al., 2012; Henderson et al., 2013; Lindholm et al., 2008; Lindholm et al., 2007; Matlik et al., 2015; Petrova et al., 2003).

Endoplasmic reticulum stress is caused by the accumulation and aggregation of misfolded proteins in the ER, which activates the unfolded protein response (UPR), an adaptive

pathway that tends to restore protein and ER homeostasis (Wang and Kaufman, 2016). Chronically activated UPR has been associated with neuronal dysfunction and cell death in neurodegenerative diseases such as PD and Alzheimer's disease (Hoozemans and Scheper, 2012; Lindholm et al., 2006). MANF regulates ER stress; moreover, ER stress regulates MANF expression and secretion *in vitro* and *in vivo* (Apostolou et al., 2008; Glembotski et al., 2012; Lindahl et al., 2014; Lindahl et al., 2017; Tseng et al., 2017). Less is known about the function of CDNF in ER stress than of MANF. In contrast to MANF, CDNF expression is not upregulated in tunicamycin-induced ER stress in the osteosarcoma U2OS cell line (Apostolou et al., 2008). CDNF, however, has been shown *in vitro* to alleviate ER stress and synaptotoxicity and thus to protect primary hippocampal neurons from Aβ oligomer-induced neurotoxicity (Zhou et al., 2016). This observation may account for the finding that CDNF overexpression in the brains of APP/PS1 transgenic animals improves long term memory (Kemppainen et al., 2015). Recombinant CDNF also downregulates activated UPR pathways *in vivo* in 6-hydroxydopamine (6-OHDA)-lesioned rat brain and *in vitro* after thapsigargin-induced ER stress in fetal mouse midbrain neurons (Voutilainen et al., 2017). Although CDNF is currently being tested in a phase I-II clinical trial in PD patients (Huttunen and Saarma, 2019), very little is known about CDNF effects *in vivo* and nothing is known about the biological role of endogenous CDNF.

To understand the physiological roles of CDNF in mammals, we generated $Cdnf^{-/-}$ mice. We found that an age-dependent loss of neurons occurs selectively in the submucosal plexus of $Cdnf^{-/-}$ mouse gut along with a slowing of GI motility (Chalazonitis et al., 2013) Age-dependent abnormalities occurred in D-amphetamine responses in $Cdnf^{-/-}$ mice, demonstrated by hyperactivity, aberrant function of the dopamine transporter (DAT), and altered dopamine release at dopaminergic axon terminals in the striatum.

2. Materials and methods

2.1. Ethics statement and mice

All experimental procedures involving mice in Finland were approved by the National Animal Experiment Board. Mice were maintained in a pathogen-free facility with a 12 h light/dark cycle and unlimited access to food (Harlan, Teklad Global, 16% protein rodent diet, 2016) and water. In all studies in which $Cdnf^{+/+}$ and $Cdnf^{-/-}$ mice were compared, we used sex-matched siblings derived from crossings of $Cdnf$ heterozygous ($Cdnf^{+/-}$) animals either in a hybrid Ola129/C57BL/6JRcc/ICR mixed genetic background or in a C57BL/6JRcc background (backcrossed for more than six generations). For behavioral studies homozygotic mice derived from heterozygotic parents were used in the breeding. For mice used in GI studies, cohorts of age-matched $Cdnf^{+/+}$ and $Cdnf^{-/-}$ mice bred from heterozygous parents were sent from the University of Helsinki to Columbia University animal facilities and were housed in an isolated room to readapt after transport for at least three days. All subsequent procedures were approved by the Animal Care and Use Committee of Columbia University. Mice were analyzed at 5 representative ages 1.5 months, 3–4 months, 5–6 months, 9–12 months and 24 months old.

2.2. Construction of Cdnf-targeted mice and animals used

CDNF positive clones of mouse BAC-129 SvEvTac RP-22 library filters (BACPAC Resources, CHORI) were identified by dot-blotting using ^{32}P-dCTP radiolabeled full-length mouse CDNF cDNA. Positive chromosomal BAC DNA clones were purchased from CHORI and amplified according to the manufacturer's instructions. To create the knock-out gene-targeting construct, 5′UTR and 3′UTR chromosomal regions (approximately 6 kb) flanking CDNF exons 2–4 were PCR amplified from 129/Svev genomic BAC clones containing CDNF genomic locus using primers with suitable restriction sites (5′UTR F *Pme*I 5′-ACT AGT TTA AAC GAG GAG ACT TGC TTC TCT GC-3′, R *Asc*I 5′-ATA TGG CGC GCC TAC AAA TGC ATT ACA TTC AGG-3′ and 3′UTR F *Not*1 5′-ATA AGC GGC CGC CGA AGA GTC ACT TGG GCT CAG G-3′, R *Not*1 5′-ATA AGC GGC CGC CCC AGC TAT CCT CTC TTT CAG ATG G-3′). PCR fragments (5′UTR 5593 bp and 3′UTR 5608 bp) were isolated from crystal violet gels and subcloned into a TOPO® XL Cloning vector (Invitrogen). Restriction analysis was used to investigate fragments; thereafter, they were digested from TOPO vectors *Pme*I/*Asc*I (5′UTR) and *Not*I (3′UTR) and cloned into a digested CIAP-treated gene replacement vector pFlexible (van der Weiden et al., 2005, Gene bank acc. Nr CR847878) containing a phosphoglycerate kinase (PGK)-driven positive/negative selection marker puromycin/tka cassette flanked by Frt and LoxP recombination sites. The functionality of Flp- and Cre-recombinase sites in the final targeting construct were tested in *E.coli* strains expressing Flp- or Cre-recombinase. Plasmids were isolated and successfully recombined plasmids were identified by restriction analysis. The targeting construct was linearized with *Cla*1, purified with a QiaexII Gel Extraction kit (Qiagen), and electroporated into IB10 (129/Ola) embryonic stem cells. ES clones were selected with puromycin for 7 days and about 200 clones were picked under a microscope and expanded. The chromosomal DNA was isolated from all clones and successful vector integration by homologous recombination was verified by real-time quantitative PCR (Loss-of Native–allele assay). Positive qPCR clones were identified by Southern blotting to ensure single integration. For Southern blotting, DNA from ES cells was digested with *EcoR*V and hybridized to a 300 bp 5′UTR ^{32}P-dCTP radiolabeled CDNF probe generated by PCR from BAC DNA using primers F 5′-AAA GGC AGA GGG AGC TAA GG-3′, R 5′-TGC ATG GTG GTT GAG TTT TG-3′. Positive ES clones generated a targeted band of 9.0 kb and a 13.6 kb band, which represents the wild-type allele. Two genetically modified ES-cell clones were karyotyped for correct chromosome number and aggregated with morula-stage pre-implantation embryos (ICR strain) at the GM mouse unit, University of Helsinki Laboratory Animal Center. The resulting chimeric mice were bred to ICR mice. Heterozygous CDNF mice with germ-line transmission of the targeted allele were obtained from both ES clones. Mice were genotyped by PCR using the following primers (see arrowheads in Fig. 1A) f2 5'-GCA GCC CCC TTT ATA GTG GG-3′, f3 5′-TCT GAG GCG GAA AGA ACC AG-3′ and r2 5′-TTG GAC ATC ACT TTC TGC CTC TC-3′. To remove the puromycin cassette, heterozygote *Cdnf^Pu/+* (Fig. 1A) mice were crossed to transgenic mice ubiquitously expressing CaqFlp recombinase (Lindahl et al., 2014). Mice were genotyped with CaqFlp primers (Fig. 1A) f 5′ and f1 5'-CAG AAC CCC AAA GAA TGC TTA GG-3′, r1 5'-GGC TCA GCA ATT AAG AGC ACA TG-3′ and r2 5′-TTG GAC ATC ACT TTC TGC CTC TC-3′.

2.3. RNA isolation, reverse transcription (RT) and quantitative (Q)PCR

RNA from tissues was isolated with TriReagent® (Molecular Research Center) or by using NucleoSpin RNA® II (Macherey-Nagel) according to the manufacturer's instructions. Reverse transcription reactions were carried out with RevertAid™ Premium Reverse Transcriptase (Fermentas UAB, Thermo Fisher Scientific Inc.), and dNTP mix, 10 mM each (Fermentas UAB), oligo(dT)15 primers, 500 μg/ml (Promega Corporation) for 40 min at 55 °C according to the manufacturer's protocol. Quantitative PCR was performed using LightCycler® 480 SYBR Green I Master Mix (Roche Diagnostics GmbH) and a Roche LightCycler® 480 Real-Time PCR System. The expression levels were normalized to the levels of β-actin in the same samples.

2.4. Primer sequences used in QPCR and RT-PCR

Primer sequences used to synthesize primers for RT-PCR and QPCR are listed in Lindahl et al., 2014 and below: *Atf*6β, Forward (F) 5′-CAG CCA TCA GCC ACA ACA AG-3′, Reverse (R) 5′-GGC ATC ACC AGC GAC ATC TT-3′, *Cdnf* exons 1–2 F 5′- CCG AGG GCT GAC TGT GAA G-3′, R 5′-GCA GAA AAG TCT ATG CCT CTG C-3′, *Cdnf* full (used in Fig. 1C) F 5′-ACC ATG CGG TGC ATC AGT CCA ACT-3′, R 5′-GAG CTC CGT TTG GGG GTA TAT C-3′. *Manf* Exons 3–4 (used in Fig. 6J and Supplemental Fig. 2B) F 5′- GAC AGC CAG ATC TGT GAA CTA AAA-3′, R 5′- TTT CAC CCG GAG CTT CTT C-3′.

2.5. Immunocytochemistry and quantitation of neurons

2.5.1. Optical density of TH- and DAT-immunoreactive fibers in the striatum

—To analyze the striatal innervation from substantia nigra dopamine neurons, TH- and DAT-immunoreactive fibers were analyzed in the striata of *Cdnf*$^{-/-}$ and *Cdnf*$^{+/+}$ littermates. The striata from 4% formaldehyde (prepared from paraformaldehyde [PFA]) fixed and paraffin-embedded brains were cut into 5-μm sections and 5 to 6 sections spanning the striatum were selected for immunostaining. For analyzing MANF expression in the gut, parts of the duodenum, jejenum ileum and colon of WT adult mice were formaldehyde-fixed, embedded in paraffin and sectioned at 5 μm. Antigen retrieval was carried out by boiling sections in 10 mM citrate buffer, pH 6, for 10 min. Endogenous peroxidase was inactivated by incubation with 0.6% H_2O_2 in Tris-buffered saline (TBS). Sections were blocked with 1.5% goat serum in TBS with 0.1% Tween 20 and incubated overnight with antibodies to TH (dil. 1:1000, Millipore, #MAB318, RRID:AB_2201528), DAT (dil. 1:1000, Millipore, #MAB369, RRID:AB_2190413) or MANF (dil. 1:300, Icosagen, #310–100, batch A12ManfPab-005, RRID: AB_1135308). After incubation with biotinylated secondary antibodies (1:200, Vector, BA-2000, BA-9400), immunostaining was visualized with 3′,3′-diaminobenzidine chromogen amplified by avidin-biotin complex formation (ABC kit, Vector). To decrease the background, sections were scanned with an automated scanner (3DHistech, Budapest, Hungary; the scanning service was provided by the Institute of Biotechnology, University of Helsinki; http://www.biocenter.helsinki.fi/bi/histoscanner/index.html), and the images were converted to a 16-bit gray scale. The corpus callosum, which is devoid of TH or DAT, was used to estimate nonspecific background staining. The

integrated densities divided by area from the obtained images were analyzed with ImageJ (NIH) software.

2.5.2.   Stereological assessment of TH-reactive neurons in substantia nigra

—For immunocytochemistry, mice were perfused transcardially with phosphate-buffered saline (PBS, pH 7.5), 4% formaldehyde (from PFA) and tissues were postfixed with 4% formaldehyde (from PFA) for at least 12 h. Tissues were cryoprotected with 20% sucrose in PBS. To assess the total number of TH+ neurons in the SNpc, we used 40 μm free-floating cryosections, which were stained with antibodies to TH (Millipore, #MAB318), and visualized with 3′,3′-diaminobenzidine. Three slides from each animal from the same regions of the SNpc, were selected for quantitation with a Stereo Investigator platform (MicroBrightField) attached to an Olympus BX1 microscope as described previously (Mijatovic et al., 2007; Voutilainen et al., 2009). To quantify dopaminergic neurons in that SNpc and ventral tegmental area (VTA), the 5-μm-thin paraffin sections from the SN were immunostained with antibodies to TH (dil. 1:1000, Millipore, #MAB318) and counterstained with hematoxylin. Images were captured with 3DHistech scanner; a region of the SNpc or the VTA was cropped and TH-immunoreactive neurons were counted with a Matlab algorithm, which recognizes cells based on their intensity and size (Penttinen et al., 2016). Intensity threshold was determined separately for each section, but the threshold for the cell size was kept constant. Neurons in the SNpc from one hemisphere and the VTA region from both hemisperes were counted in 3 to 4 sections per animal and represented as an average.

2.5.3.   Immunohistochemistry and quantitation of neurons of the small intestine and colon

—Methods were similar to those previously described (Chalazonitis et al., 2008; Chalazonitis et al., 2011; Pham et al., 1991). Briefly, mouse small intestine or colon were isolated, their lumen was flushed with Krebs solution, and tissues were fixed with phosphate-buffered 4% formaldehyde (from PFA) at pH 7.4. Laminar preparations containing the myenteric (MyP) or submucosal (SMP) plexuses were then dissected from duodenum, jejunum, ileum, and colon. Neurons were identified with biotinylated monoclonal antibodies to HuC/D (Thermo Fisher Scientific, Molecular Probes Cat# A-21272, RRID: AB_2535822);) or a polyclonal anti-human neuronal nuclear antigen ANNA-1 [gift of Vanda Lennon, Mayo Clinic, Rochester MN at 1:40000; King et al., (1999)] that cross-reacts with mouse neurons (Margolis et al., 2016). Sites where these primary antibodies were bound were visualized, respectively, with streptavidin Alexa 594 (Thermo Fisher Scientific, Molecular Probes, diluted 1:400) and donkey anti-human secondary antibodies coupled to Alexa 488 (Thermo Fisher Scientific, Molecular Probes; diluted 1:400).

2.5.4.   Neuronal quantitation

—Neurons in whole mounts of laminar preparations containing the SMP were examined with an upright fluorescence microscope (Leica DMRXA2), using a 40× objective. Neurons were counted by an observer who was blinded to the genotype of the tissue. Three independent determinations were made for each region of gut in each animal. Neuronal cell bodies were enumerated in contiguous, non-overlapping rectangular fields, which were scanned across the width and length of each whole mount. A

single measurement was defined as the sum of neurons in 10 fields covering an area of 1.25 mm^2. The numbers of measurements ranged from 71 to 80 (in juvenile), 60 to 70 (in young adult) and 99–102 (in mature adult) animals. Because the total number of enteric neurons varies as a function of animal age, neuronal density was expressed both as neurons per mm^2 and as % wild-type at each age examined. Immunofluorescence images were obtained with a digital CCD camera (Retiga Exi), mounted on a Leica DM 6000B microscope. Images were obtained with computer assistance (Volocity 6.3 software; Improvision/PerkinElmer Life and Analytical Sciences). Adobe CS5 Photoshop software was used to assemble montages.

2.5.5.   Glial quantitation—Cross-sections from ileum and colon of juvenile *Cdnf*$^{+/+}$(15–20 measurements) and *Cdnf*$^{-/-}$ (16–24 measurements) animals, cut in a cryostat-microtome, were processed to demonstrate the immunoreactivity of the glia marker, S100β (rabbit polyclonal antibodies dil 1:500; DAKO, # Z0311; RRID:AB_10013383) and the nuclear DNA marker, bisbenzimide (dil 1:1000; Hoechst 33258, Thermo Fisher Scientific, #H3569; RRID:AB_2651133). The density of glia in the enteric plexuses was quantified as the ratio of the fluorescence intensity of S100β-immunoreactivity (green fluorescence) to that of DNA (blue fluorescence). Computer-assistance was used to quantify fluorescence intensity (Volocity 6.3 software). Regions of interest (ROIs) were delineated within the sections such that myenteric and submucosal plexuses, as well as the deep muscle plexus and the nerves within the muscularis externa were included.

2.5.6.   Neuronal apoptosis—Segments of ileum and colon from 1.5 month-old animals were prepared to obtain optically cleared whole mounts of the entire bowel wall (Rao et al., 2015; Wilson et al., 2011). Tissues (1.5 cm in length) were cleaned, the mesentery was removed, the bowel was opened longitudinally, pinned flat, and fixed for 2 h at 4 °C. Neurons were identified with ANNA-1 antibodies (diluted 1:40,000) and apoptotic cells were detected with an early marker of apoptosis, the phosphorylated histone H2A.X (PH2A.X) using rabbit monoclonal antibodies (Cell Signaling Technology, Cat# 9718, RRID: AB_2118009) diluted 1:200, for 48–72 h (Holubec et al., 2005; Lu et al., 2006; Rogakou et al., 2000; Wilson et al., 2011). Sites of primary antibody binding were detected with species-specific goat secondary antibodies coupled, respectively to Alexa 488 or Alexa 594 (Invitrogen; diluted 1:500). Preparations were washed, dehydrated with graded methanol, and optically cleared with benzyl alcohol–benzyl benzoate (BABB). Neurons in the optical planes of the submucosal and myenteric plexuses were quantified as described above except that a 20 × objective was employed and neurons were counted in a 3-dimensional volume of 0.09 mm^3 of tissue; the numbers of such individual measurements ranged from 65 to 91.

2.5.7.   Degenerating neurons—To identify enteric neurons which were in the process of degenerating rather than undergoing apoptosis, histochemical staining using Fluoro-Jade C (FJC) was applied as a specific marker (Bian et al., 2007; Ehara and Ueda, 2009; Hoang et al., 2009; Schmued et al., 1997). Sections of frozen blocks of ileum and duodenum isolated from gut of juveniles *Cdnf*$^{-/-}$ and *Cdnf*$^{+/+}$ littermates were first treated for fluorescence immunocytochemistry with human ANNA-1 antibodies (1:10,000) followed with DyLight 594 Goat anti-human IgG (1:300) to label all neurons. Sections were then post-fixed,

exposed to $KMnO_4$, then transferred to a solution of FJC (0.0001% in acetic acid) and incubated for 10 min. The sections were then rinsed in deionized H_2O and mounted in an acidic mounting medium. Subsets of FJC-labeled neurons were identified with green fluorescence and analyzed in both myenteric and submucosal plexuses. Quantitation of FJC-labeled neurons was expressed as % of total ANNA-1 labeled neurons in each plexus. Proportions of FJC-labeled neurons per section were obtained from 8 (duodenum), 12 (ileum), 20 (colon) sections of $Cdnf^{+/+}$ and from 11 (duodenum), 15 (ileum), 27 (colon) sections of $Cdnf^{-/-}$ littermates. Data were expressed as the means ± standard error.

2.5.8.   Density of autophagosomes—To quantify the density of autophagosomes, whole mounts containing the SMP were prepared from mature adult (9–12 months) mice. Rabbit antibodies to microtubule-associated protein 1A/1B-light chain 3 (LC3; Novus Biologicals, Cat# NB100–2331SS, RRID: AB_791016) diluted 1:100–1:75) were used to identify autophagosomes (Hung et al., 2014). ANNA-1 was employed as a neuronal marker. Sites of bound primary antibodies were identified, respectively, with Alexa 488-labeled goat anti-rabbit and donkey Alexa 594-labeled anti-human secondary antibodies. A 100× objective was used to identify and quantify LC3-immunoreactive puncta in the cell bodies of identified neurons. For quantitation, the sum of these puncta was determined within a field of cytoplasm narrowed to 7.85 μm^2. This sum per cell soma was defined as one count and a single measurement was defined as the mean of 10 counts. Twelve such measurements were made from each type of mouse and means were statistically compared. Background counts of puncta were ascertained in similar preparations that were treated identically, except that primary antibodies to LC3 were omitted. Again, counts were obtained while blinded to the genotype of the tissue. To validate and confirm immunocytochemical observations, neurons were also examined electron microscopically. For this purpose, gut was fixed by immersion in a freshly prepared mixture of 4% formaldehyde and 0.2% glutaraldehyde in 0.1 M phosphate buffer, pH 7.4. Tissues were postfixed with 2% OsO_4 for 1 h, stained *en bloc* with 5% aqueous uranyl acetate, dehydrated in a graded series of ethanols, cleared with propylene oxide, and embedded in Epon 812 (Ted Pella, Redding, CA). Sections (80 nm) were collected on copper grids and examined with a JEOL 1200EX electron microscope. The density of morphologically identified autophagosomes in each electron micrograph was normalized to 10^{-3} μm^2 of ganglionic area. These data were also expressed as the % determined in $Cdnf^{+/+}$ mice. Measurements were made in 25–55 individual neurons in each plexus of ileum and colon in $Cdnf^{+/+}$ and $Cdnf^{-/-}$ mice.

2.6.   Western blot analysis

Tissues were homogenized in lysis buffer (100 mM Tris-HCl, pH 7.5, 300 mM NaCl, 4 mM EDTA, 2% BSA, 0.2% Triton X-100, 2 mM PMSF, 1 mM sodium orthovanadate, protease cocktail inhibitor (Complete, Mini EDTA, Boehringer Mannheim), incubated on ice for 15–30 min, and centrifuged at 13000 rpm for 30 min. For detection of CDNF protein, 1 M HCl was added to the supernatant (pH < 2), and the samples were incubated for 30 min on ice. The pH of the samples was adjusted to pH 7.6 using 1 M NaOH. Protein content was determined by Bradford protein assay (Bio-Rad). Aliquots of supernatant were mixed in Laemmli buffer. Proteins were separated by SDS-PAGE and transferred to nitrocellulose membranes. Immunoblot analysis using antibodies against CDNF (1:1000,

used as determined in (Lindholm et al., 2007) and actin (1:1000, Sigma, Cat# A3853, RRID: AB_262137, Clone AC40) were used to identify the protein of interest. Blots were developed using chemiluminescence ECL Blotting Substrate (Pierce, Thermo Scientific). DA and its metabolites levels were determined in brain samples by using HPLC as previously described (Airavaara et al., 2006; Kumar et al., 2016).

2.7. Analysis of blood samples

Blood glucose levels in randomly fed animals were analyzed using a glucometer (Accucheck Aviva Glucometer, Roche Diagnostics). For measurement of constituents of blood, sera were collected by centrifugation of blood collected from heart of freshly euthanized animals and frozen at −80 °C until used. Clinical chemistry analyses from serum samples were performed with an automatic analyzer (Konelab v.7.1.1) according to the manufacturer's instructions in the Central Laboratory of the Faculty of Animal Medicine, Department of Equine and Small Animal Medicine, University of Helsinki.

2.8. Behavioral testing

Novelty-induced locomotor activity in open field (OF): Mice were released in the corner of a novel open field arena (30×30 cm, Med Associates). Horizontal and vertical activity was recorded for one hour (light intensity ~150 lx). The peripheral zone was defined as a 6 cm wide corridor along the wall of the arena.

Forced swim test (FST).—Mice were placed for 6 min in a glass cylinder (diameter 18 cm, height 25 cm) filled with water (23 ± 1 °C) to a height of 15 cm. The time of immobility was defined as passive floating with the animal motionless or only slightly moving its tail or a hind limb. The time of activity was defined as struggling, climbing, or swimming using all four paws. Times of immobility and activity were measured at 2 min intervals.

Amphetamine-induced locomotor activity: Mice were habituated in an open field arena for 30 min. D-amphetamine (3 mg/kg) was then administered intraperitoneally and the mice were returned immediately to the open field for recording of activity during the subsequent 90 min.

GBR 12909-induced locomotor activity: 11 month-old male $Cdnf^{-/-}$ mice with wild-type controls in an ICR background were habituated in an open field arena for 30 min. Mice were injected with a selective dopamine reuptake inhibitor, GBR 12909 (20 mg/kg), placed back into the arena and activity was monitored for the following 120 min.

2.9. Fast-scan cyclic-voltammetry

Striatal slices (300 μm thickness) were cut on a vibrating microtome in ice-cold cutting saline containing: 125 mM NaCl, 2.5 mM KCl, 26 mM NaHCO$_3$, 0.3 mM KH$_2$PO$_4$, 3.3 mM MgSO$_4$, 0.8 mM NaH$_2$PO$_4$, 10 mM glucose. Slices were allowed to recover for 1–2 h at 35 °C in oxygen-bubbled (95% O$_2$, 5% CO$_2$) recording saline containing: 125 mM NaCl, 2.5 mM KCl, 26 mM NaHCO$_3$, 0.3 mM KH$_2$PO$_4$, 2.4 mM CaCl$_2$, 1.3 mM MgSO$_4$, 0.8 mM NaH$_2$PO$_4$, 10 mM glucose. Slices were then transferred into a recording chamber that was perfused with 35 °C oxygen-bubbled recording saline. When

D-amphetamine was studied, the drug was added to the perfusing solution (5 μM) after a stable baseline of stimulated transients had been reached. Recordings were carried out with cylindrical 5 μm carbon fiber electrodes and DA release was stimulated electrically using a bipolar stainless-steel electrode. Triangular voltage ramps from a holding potential of −450 mV to +900 mV over 9 ms (scan rate of 300 mV/ms) were applied to a carbon fiber electrode at 100 ms intervals. Current was recorded with an Axopatch 200B amplifier (Molecular Devices) filtered with 5 kHz low-pass Bessel filter and digitized at 40 kHz (ITC-18 board). Triangular wave generation and data acquisition were controlled and the recorded transients were characterized by a computer routine in IGOR Pro (WaveMetrics) written by Eugene Mosharov (http://sulzerlab.org/download.html). Background-subtracted cyclic voltammograms obtained with a known concentration (1 μM) of DA solution were used to calibrate the electrodes and to identify DA.

2.10. Experimental design and statistical analyses

The overarching design of the studies was to analyze the effects of CDNF on the midbrain and the ENS in juvenile, young adult, mature and aged animals. For studies of the brain, significance of differences between two groups was analyzed by Student's unpaired two-tailed *t*-test using Microsoft Excel software. Differences between more than two groups were calculated by one-way analyses of variance (ANOVA) followed by appropriate post-hoc analysis, using the SPSS Inc. PASW Statistics 18 program. For statistical analysis of quantified numbers of dopaminergic neurons, Stereoinvestigator software was employed and a t-test with Welch's correction was used to compare groups. Results are expressed as means ± standard error of the mean and were considered significant if $p < .05$. For quantitation of neuronal densities in enteric plexuses, and autophagosome density results, GraphPad Prism software (version 7.0) was used to calculate means and standard errors as well for tests of statistical significance. Means were compared with Students unpaired *t*-test and multiple means were compared with one-way ANOVA. Tukey or Bonferroni-Dunn methods were employed for post-hoc comparisons. For behavioral studies, factorial ANOVA with genotype and strain as independent variables were used. Locomotor activity in an open field was analyzed by repeated measures ANOVA for 5-min intervals with genotype and treatment as independent variables. Voltammetry data was analyzed by GraphPad Prism software (version 6.0), using two-way ANOVA (age and genotype) and Tukey's multiple comparisons. Statistical details of individual experiments are presented with the relevant results in the figure legends.

3.   Results

3.1.   Cdnf⁻/⁻ mice are viable, fertile, and do not show an obvious growth defect

We generated conventional $Cdnf^{-/-}$ mice by replacing exons 2–4 in the endogenous $Cdnf$ locus with a targeting construct containing a PGK-driven positive/negative selection marker cassette in between the 5′UTR and 3′UTR chromosomal homology arms (Fig. 1A). The resulting heterozygous $Cdnf^{Pu/+}$ mice were viable and fertile; however, growth of homozygous $Cdnf^{Pu/Pu}$ embryos was delayed and premature embryonic lethality occurred before embryonic day (E) 12, probably due to a defect in chorioallantoic fusion, which caused a hydropic allantois and a failure in umbilical cord formation (not shown).

The puromycin cassette was therefore removed from the locus by crossing heterozygote *Cdnf*^{+/−} mice with ubiquitous Flp-recombinase expressing mice (Fig. 1A). The resulting homozygous *Cdnf*^{−/−} mice were viable and fertile, suggesting that the puromycin cassette in the homozygous *Cdnf*[Pu/Pu] mice interfered with vital genes (not shown). We continued our analysis with the viable *Cdnf*^{−/−} mice, lacking the puromycin cassette and exons 2–4. Absence of transcripts encoding CDNF and protein from tissues of *Cdnf*^{−/−} mice was verified by semi-quantitative RT-PCR (Fig. 1C) and Western blotting (Fig. 1D). There was no significant difference in weight-gain between mice of different genotypes measured weekly from post-natal day 3 (P3) until 3 months of age (Fig. 1E). No difference in weight between genotypes was found in 1 year-old mice of either inbred C57BL/6JRcc or ICR/mixed genetic background (Fig. 1F–G). Clinical biochemistry parameters in sera from *Cdnf*^{−/−} mice did not differ from WT mice (Fig. 1H). Because *Manf*^{−/−} mice suffer from diabetes mellitus (Lindahl et al., 2014), we measured blood glucose levels from *ad libitum* fed 1 year-old animals. *Cdnf*^{−/−} mice in both mixed and C57BL/6 background had normal blood glucose levels (Fig. 1I). Finally, organ weights in *Cdnf*^{−/−} mice were not significantly different from those of *Cdnf*^{+/+} mice measured in 2 year-old animals. We can therefore conclude that CDNF ablation in mice does not cause gross phenotypic defects.

3.2. Age-dependent hypoplasia and non-apoptotic neuronal degeneration occurs in the submucosal plexus but not in the myenteric plexus of mice lacking CDNF

Transcripts encoding *Cdnf* are expressed in the murine gut of adult wild-type mice (Lindholm et al., 2007). We found, that transcripts encoding CDNF were present in the stomach, intestine and colon of mice as early as postnatal day 7 (P7) (Fig. 2A). We have previously reported that CDNF transcripts are expressed in enteric neural crest-derived cells as early as E16 (Chalazonitis et al., 2013). These observations suggest that CDNF is expressed during a period when ENS neurogenesis, which declines after P21, is active (Pham et al., 1991; Chalazonitis et al., 2013). Because CDNF is expressed in the bowel, we determined the effect of its deletion on the numbers of neurons in the ENS at different ages. The densities of neurons (neuronal numbers/unit area) in the distal small intestines of *Cdnf*^{+/+} and *Cdnf*^{−/−} mice were compared in 1.5 month-, 3 month-, and 9–12 month-old mice (Fig. 2B–D). These data were also expressed as % of change in neuronal number (Fig. 2B). In both *Cdnf*^{+/+} and *Cdnf*^{−/−} mice, neuronal density was greater in 3 month-old than in 1.5 month-old mice, reflecting the post-natal maturation of the ENS (Fig. 2B–D; compare D_1 with D_2 and D_4 with D_5). Neuronal density declined in 9–12 month-old mice, reflecting the known (Liu et al., 2009) age-dependent loss of enteric neurons (Fig. 2B and D; compare D_3 with D_6). Neuronal density, in *Cdnf*^{−/−} mice, however, was significantly lower than that of *Cdnf*^{+/+} animals at every age examined. This hypoplasia of the submucosal plexus (SMP) of *Cdnf*^{−/−} mice was apparent in 1.5 month-old juvenile mice and persisted to adulthood (Fig. 2B). Similar data were obtained in the jejunum (not shown). The difference between *Cdnf*^{+/+} and *Cdnf*^{−/−} mice was greater in 1.5 month- and 3 month-old mice, than in 9–12 month-old; therefore, the age-related loss of neurons was more accentuated in *Cdnf*^{+/+} than in *Cdnf*^{−/−} animals, (Fig. 2B; compare D_2 with D_3; D_5 with D_6). These data are consistent with the idea that the CDNF gene deletion must affect ENS development and that CDNF has a strong protective effect on the submucosal neurons in post-natal life and continues to

maintain them with age; alternatively, CDNF may promote the development of neurons that are especially susceptible to loss as a function of age.

Because the deletion of CDNF appeared to exert a greater effect on numbers of neurons in 1.5 month-old than 9–12 month-old mice, we tested the hypothesis that the deletion leads to apoptosis of enteric neurons in 1.5 month-old animals. To do so, we quantified both the numbers of neurons and the proportion that are apoptotic in both enteric plexuses of mice at 1.5 months of age. Both small and large intestine were examined. In these experiments, the gut wall was not dissected into laminae but was optically clarified and examined as an intact whole mount. The packing density of submucosal neurons (demonstrated with antibodies to ANNA-1) was again found to be significantly lower in $Cdnf^{-/-}$ mice than in $Cdnf^{+/+}$ mice (Fig. 3A, B). Neurons undergoing apoptosis were identified using antibodies to PH2A.X, a marker of double-DNA strand brakes and early apoptosis as well as DNA repair and replication (Holubec et al., 2005; House and Koch, 2014; Lu et al., 2006; Rogakou et al., 2000). Although rare apoptotic neurons were encountered in a minority of both $Cdnf^{+/+}$ and $Cdnf^{-/-}$ mice (Fig. 3B insets), the proportion of neurons undergoing apoptosis was not significantly different from zero in any of the animals examined (Table 1).

The packing densities of myenteric neurons in $Cdnf^{-/-}$ mice did not differ significantly from those of $Cdnf^{+/+}$ animals and again (Fig. 3C, D), the number of apoptotic neurons was similar in all animal genotypes (Table 1). These data suggest that although a deficiency in neuronal density is detectable in $Cdnf^{-/-}$ mice as early as 1.5 months of age, there is no alteration of the proportion of neurons undergoing apoptosis in the $Cdnf^{-/-}$ animals. Few apoptotic neurons were detected in either the ileum or colon of both $Cdnf^{+/+}$ and $Cdnf^{-/-}$ mice (Table 1).

Since no increased apoptosis could be demonstrated in neurons of the submucosal plexus in $Cdnf^{-/-}$ mice, slow degeneration could be an alternative mechanism to explain their declining numbers. To test this possibility, histochemical analysis using a specific neuronal degeneration marker, Fluoro-Jade C (FJC), was carried out on sections of duodenum, ileum, and colon (proximal and distal) from 1.5 month-old $Cdnf^{+/+}$ and $Cdnf^{-/-}$ mice. FJC-labeled neurons were quantified as proportions of total neurons (labeled with ANNA-1) per section in both submucosal and myenteric plexuses. In the submucosal plexus, the proportions of FJC-labeled neurons were significantly higher in $Cdnf^{-/-}$ than in $Cdnf^{+/+}$ mice in duodenum (Fig. 4A; C–H) ileum (Fig. 4B; I–K) as well as in colon (Fig. 4C). In contrast, the proportions of degenerating myenteric neurons in the duodenum (Fig. 4A) and ileum (Fig. 4B), were significantly lower than in the submucosal plexus; however, the proportions of myenteric degenerating neurons in $Cdnf^{-/-}$ mice were not different from those in $Cdnf^{+/+}$ animals in all three regions of the gut (Fig. 4A, B, C). These data suggest that neuronal degeneration, rather than apoptosis probably contributes to the selective hypoplasia of the submucosal plexus that occurs in $Cdnf^{-/-}$ mice.

3.3. Autophagy in enteric neurons is greater in Cdnf$^{-/-}$ than in Cdnf$^{+/+}$ mice

The smaller number of submucosal neurons in $Cdnf^{-/-}$ than in $Cdnf^{+/+}$ mice could be due to diminished neuronal differentiation or survival. An effect on either would be likely to occur if neurons or their precursors in $Cdnf^{-/-}$ mice were to be more highly stressed than

in $Cdnf^{+/+}$ animals. Autophagy is a common response of cells to stress and dysregulation of autophagic mechanisms has been associated with PD (Lynch-Day et al., 2012; Michel et al., 2016). We thus reasoned that the occurrence of autophagy would increase in the enteric neurons of $Cdnf^{-/-}$ mice if they were more susceptible to stress than those of $Cdnf^{+/+}$ animals. Antibodies to LC3, which is a marker for autophagosome formation, and the neuronal marker, ANNA-1, were applied simultaneously to laminar preparations of ileum containing the submucosal plexus to quantify autophagy in cells identified as neurons. Studies were carried out with $Cdnf^{+/+}$ (Fig. 5A–C) and $Cdnf^{-/-}$ (Fig. 5D–F) 9–12 month-old mice. The density of LC3-immunoreactive puncta/neuron was significantly greater in $Cdnf^{-/-}$ than in $Cdnf^{+/+}$ animals (Fig. 5G). These observations are thus consistent with the idea that the amount of autophagy in submucosal neurons of $Cdnf^{-/-}$ mice exceeds the constitutive amount seen in submucosal neurons of $Cdnf^{+/+}$ animals. EM was employed to extend observations made at the light microscopic level with LC3 immunoreactivity (Fig. 5J–M). EM has been shown to be more sensitive and to have a better resolution than immunocytochemistry for the detection of autophagic figures in cells (Eskelinen et al., 2011). Both ileum and colon were examined and autophagic figures were identified and quantified in submucosal and myenteric neurons of ileum and colon. Early autophagosomes have a double limiting membrane; however, the double membrane is lost when the structures fuse with endosomes or lysosomes. Late autophagic figures can be identified by their content of cytoplasmic material or organelles. Although the density of autophagosomes in the myenteric plexus of the $Cdnf^{-/-}$ ileum was not significantly different from that of $Cdnf^{+/+}$ animals, the density of autophagosomes in the submucosal plexus of $Cdnf^{-/-}$ mice was significantly greater than that of their $Cdnf^{+/+}$ counterparts (Fig. 5H, J, K). In contrast, the density of autophagosomes was significantly greater in both plexuses of the $Cdnf^{-/-}$ than of the $Cdnf^{+/+}$ colon (Fig. 5I, L, M). These results are compatible with the previously shown neuroprotective properties of CDNF and suggest that its protective effects are more evident in the submucosal plexus and in the colon, where neurons may be more stressed than in the myenteric plexus of the small intestine.

3.4. Density of glia is not different in the enteric plexuses of Cdnf^−/− mice and Cdnf^+/+ mice

Sections from 1.5 month-old animals were analyzed to evaluate the density of glia. Glial density was taken as the ratio of S100 β fluorescence to that of DNA demonstrated with bisbenzimide. Measurements included glia in the submucosal and myenteric plexuses as well as those in the muscle layers and the deep muscle plexus. Glial density was not found to be significantly different in either the ileum or colon of $Cdnf^{-/-}$ and $Cdnf^{+/+}$ animals (Supplemental Fig. 1).

3.5. The general architecture of midbrain dopaminergic neurons of Cdnf^−/− mice is similar to that of Cdnf^+/+ mice at different ages

Because GI abnormalities occur in mature adult $Cdnf^{-/-}$ mice (Chalazonitis et al., 2013) similarly to those seen in PD patients before the onset of movement disorders, we analyzed nigrostriatal dopaminergic neurons. TH and DAT immunoreactivity were used to analyze neurite densities and number of nigrostriatal dopaminergic neurons. In contrast to the neurodegeneration of enteric submucosal neurons that already occurs in 1.5 month old

mice, the number of neurons in the SNpc and the optical density of TH+ and DAT+ striatal neurites at the age of 3 months were similar in $Cdnf^{-/-}$ and $Cdnf^{+/+}$ mice (Fig. 6A–D). Neuronal numbers (Fig. 6E) and striatal neurites (Fig. 6F) did not differ between genotypes even in 1 and 2 year-old mice. There were no differences in the concentrations of DA, 4-dihydroxyphenylacetic acid (DOPAC) or homovanillic acid (HVA), 5-hydoxytryptamine (5-HT) or 5-hydroxyindoleacetic acid (5-HIAA) measured with HPLC in the striatal tissue of one-year old $Cdnf^{-/-}$ and $Cdnf^{+/+}$ mice (Fig. 6G).

Because MANF deficiency in pancreatic beta cells leads to chronically elevated UPR (Lindahl et al., 2014) and exogenously added CDNF can modulate ER stress in animal models of PD (Voutilainen et al., 2017), we used qPCR to measure the ER stress levels of the SN and striatum of 9–12 month-old $Cdnf^{+/+}$ and $Cdnf^{-/-}$ mice. No difference was detected in the levels of transcripts encoding typical UPR genes in the SN (Fig. 6H) and striatum (Fig. 6I) of $Cdnf^{-/-}$ and $Cdnf^{+/+}$ mice. To investigate whether upregulation of MANF compensates for the loss of CDNF in the brains of $Cdnf^{-/-}$ mice, we measured transcripts encoding *Manf*. Levels of transcripts encoding *Manf* were not significantly different in the SN or striata of $Cdnf^{-/-}$ mice from those in $Cdnf^{+/+}$ mice (Fig. 6J). MANF is highly expressed at the base of epithelial crypts, particularly in small intestinal regions (Danilova et al., 2019; Supplemental Fig. 2A). This region of the crypt contains Paneth cells and Lgr5-expressing stem cells. Lower levels of MANF expression were found in ganglia of the submucosal and myenteric plexuses in the gut than in the epithelium (Supplemental Fig. 2A). The *Manf* mRNA levels in the duodenum of 1.5 year-old $Cdnf^{-/-}$ mice were similar to those of $Manf^{+/+}$ mice (Supplemental Fig. 2B), indicating no compensatory upregulation of MANF expression occurs in the gut of $Cdnf^{-/-}$ mice. In conclusion, we were not able to detect overt neurodegeneration or changes similar to those seen in the ENS or in PD in the brains of $Cdnf^{-/-}$ mice.

3.6. Amphetamine-induced hyperlocomotion is enhanced in mice lacking CDNF

We next determined whether dopaminergic neurotransmission was altered in $Cdnf^{-/-}$ mice. An array of behavioral tests are routinely used to assess Parkinson-like motor and non-motor phenotypes (Taylor et al., 2010). We used a novelty-induced locomotor activity test to measure spontaneous exploration as well as a stress response in an unfamiliar environment in 7 month-old mice. Baseline activity and habituation in a novel environment were similar in $Cdnf^{-/-}$ and $Cdnf^{+/+}$ mice in both genetic backgrounds, including times spent in corners *vs* center (Fig. 7A–B). No differences were seen between genotypes in exploratory, anxiety (Fig. 7C), or depression-like (Fig. 7D) behavior.

The psychostimulatory drug, D-amphetamine, enters dopaminergic axon terminals through DAT and interferes with VMAT2-positive DA storage-vesicles by collapsing pH gradients across the vesicular membrane, eventually causing DA to be displaced from the vesicles into the cytosol. The events initiated by D-amphetamine cause DAT phosphorylation and eventually reversal of its direction of transport, thereby transporting DA from the cytosol to the synaptic cleft (Fleckenstein et al., 2007). The net effect of D-amphetamine is thus to elevate levels of extracellular DA, which prolongs dopaminergic signaling in the striatum and gives rise to increased locomotor and stereotypic activities (Yates et al., 2007). In the

amphetamine-induced locomotor activity test we observed no difference between genotypes during the initial 30 min habituation period in 4 month-old and 9 month-old mice (Fig. 7E–G). According to a two-way ANOVA analysis, however, there was significant genotype × time interaction in a mixed background in young adult mice ($F(17,306) = 1.8$, $p = .026$) and, in mature adults, in both mixed ($F(17,323) = 2.0$, $p = .010$) and C57BL/6 backgrounds ($F(17,408) = 3.8$, $p < .0001$). These data show that D-amphetamine causes hyperactivity in mice lacking CDNF. The Fisher LSD post-hoc analysis, however, revealed differences relative to genotype after D-amphetamine injections only in 7–9 month-old mice in mixed (Fig. 7F) and C57BL/6 (Fig. 7G) backgrounds ($p < .05$ at marked timepoints). In conclusion, the hyperlocomotor response to D-amphetamine was significantly greater in $Cdnf^{-/-}$ than in $Cdnf^{+/+}$ mice in two genetic backgrounds and age-groups, suggesting that the function of dopaminergic neurons is altered in the CNS of $Cdnf^{-/-}$ mice.

3.7. Age-dependent changes in the function of DA axon terminals in CDNF-deficient mice

We used fast-scan cyclic voltammetry in acute striatal slices to study the kinetics of DA release and reuptake and the effects of D-amphetamine on dopaminergic axon terminals of the dorsal striatum. The amounts of DA released were similar in $Cdnf^{+/+}$ and $Cdnf^{-/-}$ mice (Fig. 8A); nevertheless, the DA transients in 6 month-old $Cdnf^{-/-}$ mice were wider, that is, their half width (width at half maximum, T ½) was longer in $Cdnf^{-/-}$ than in $Cdnf^{+/+}$ animals. The DA transients in 6 month-old $Cdnf^{-/-}$ mice were also significantly wider than in 9–12 month-old $Cdnf^{-/-}$ mice (Fig. 8A). These findings suggest that the DA re-uptake by DAT was slower in $Cdnf^{-/-}$ mice at 6 months of age, but this difference between genotypes disappeared during aging.

Perfusing striatal slices with D-amphetamine, causes DA to redistribute out of synaptic vesicles and DAT eventually to transport in reverse and to release presynaptic DA, which creates a large extracellular DA signal. In a voltammetry recording, these events are seen as a reduction in fast electrically-stimulated, exocytotic DA transients and as a slow, but large increase in background DA levels, caused by DAT-mediated DA efflux (Fig. 8B). Even though the levels of the D-amphetamine-induced, DAT-mediated slow DA efflux seemed quite variable between recordings, we found that the peak DA concentrations reached were higher in $Cdnf^{-/-}$ mice especially in 9–12 month-old animals (Fig. 8C). Interestingly, after beginning the D-amphetamine perfusion, the reversal of DAT also occurred at an earlier time point in 9–12 month-old $Cdnf^{-/-}$ mice than in 6 month-old $Cdnf^{-/-}$ mice. This same tendency towards faster DAT reversal in older animals, however, was seen also in $Cdnf^{+/+}$ mice; therefore, there was no difference in time to DAT reversal between genotypes (Fig. 8C). Reduction of the stimulated exocytotic DA release happened at a similar time course and to a similar extent in both genotypes at both ages (data not shown), indicating unaltered kinetics of D-amphetamine uptake into terminals and its vesicular effects in $Cdnf^{-/-}$ mice. Our voltammetry findings suggest that the high sensitivity to D-amphetamine-induced locomotor activation in $Cdnf^{-/-}$ mice can be explained by a more pronounced D-amphetamine-induced DAT reversal in the dorsal striatum of these animals.

To test this hypothesis, we administered GBR 12909 to 1 year-old $Cdnf^{-/-}$ mice. GBR 12909 is a more selective DAT inhibitor than is D-amphetamine but GBR 12909 is unable

to reverse the direction of DAT-mediated transmembrane transport. When given GBR 12909, the mice became activated, as shown by increased locomotor activity in an open field; however, in contrast to D-amphetamine-induced hyperlocomotion, there was no difference between genotypes (Fig. 8D). This finding supports the hypothesis that in *Cdnf*−/− mice the hypersensitivity to D-amphetamine-induced reversal of DAT explains the phenotype of the hyperlocomotion seen after D-amphetamine administration.

4. Discussion

In contrast to the poor survival, severe growth defect, and diabetes of *Manf*−/− mice (Lindahl et al., 2014), *Cdnf*−/− mice are viable, fertile and, in their normal environment, display no gross defects. An age-dependent loss of enteric neurons, however, occurs in the submucosal plexus of *Cdnf*−/− mice, resulting in slower GI motility (Chalazonitis et al., 2013). In contrast glia density associated with the myenteric and submucosal plexuses is not affected in *Cdnf*−/− mice indicating that the submucosal neurons are impacted selectively. Autophagy, moreover, is enhanced in neurons of both plexuses of mature adult *Cdnf*−/− animals. D-amphetamine-induced hyperactivity was also greater in *Cdnf*−/− than in *Cdnf*+/+ mice, probably because of altered DAT function in the midbrain of *Cdnf*−/− animals.

CDNF is expressed in stomach, small and large intestines as early as P7 (as well as in the neural crest-derived precursors of enteric neurons at E16), a time when neurogenesis is highly active in the developing murine bowel (Chalazonitis et al., 2008; Chalazonitis et al., 2013; Pham et al., 1991). The expression of CDNF is restricted to neurons in the ENS of mice (Chalazonitis et al., 2013). The early timing of CDNF expression is consistent with the idea that CDNF plays a role in ENS development, which is supported by the observation that 1.5 month- and 3 month-old *Cdnf*−/− mice have fewer submucosal neurons than their *Cdnf*+/+ littermates. The effect of CDNF deletion, which also included enhanced and selective degeneration of submucosal neurons, persisted in 9–12 month-old mice. In contrast to the submucosal plexus, the density of myenteric neurons was not significantly changed by the deletion of CDNF in either the ileum or colon. It is not clear why the submucosal plexus should be so dependent on CDNF. Submucosal neurons arise later than myenteric neurons during ontogeny (Chalazonitis et al., 2008; McKeown et al., 2001; Pham et al., 1991) and their development depends on a secondary migration of precursors from the myenteric plexus (Jiang et al., 2003; Payette et al., 1984; Ratcliffe et al., 2008), which could be influenced by CDNF. The chemically-defined phenotypes of submucosal neurons are also different from those of the myenteric plexus (Mongardi Fantaguzzi et al., 2009) and dopaminergic neurons are more abundant in the submucosal than in the myenteric plexus (Li et al., 2004, 2011).

The deletion of CDNF did not increase the number of apoptotic neurons in either enteric plexus. As has been noted previously (Chalazonitis et al., 2012; Gianino et al., 2003), we found that apoptotic enteric neurons were vanishingly rare in the ENS of both *Cdnf*+/+ and *Cdnf*−/− 1.5 month-old mice. The deficit in submucosal neurons of *Cdnf*−/− mice thus seems not to result from apoptotic cell death. Instead, staining with FJC suggests that neurodegeneration contributes to the selective hypoplasia of submucosal neurons that characterizes *Cdnf*−/− mice. Consistent with this observation, the mechanism of decreased

dopaminergic neurons in the substantia nigra of MPTP-treated mice, has previously been shown to be the consequence of degeneration rather than apoptosis (Jackson-Lewis et al., 1995; Hung et al., 2014). Similarly, sustained activation of mitochondrial stress resulting in UPR^{MT} has been shown to induce a non-apoptotic degeneration of dopamine neurons in *C. elegans* models of PD (Martinez et al., 2017). Autophagy, furthermore, was greater throughout the ENS of 9–12 month-old *Cdnf*$^{-/-}$ mice than in *Cdnf*$^{+/+}$ animals. Because autophagy may be a cellular response to stress, these data support the idea that alleviation of stress is a function of CDNF (Voutilainen et al., 2017; Zhang et al., 2018). Taken together, these data suggest that in addition to promoting development of neurons in fetal mice (Chalazonitis et al., 2010; Chalazonitis et al., 2013), CDNF exerts a sustained protective effect on submucosal neurons in post-natal animals.

Degeneration of vulnerable enteric neurons, and slowing of GI motility (Chalazonitis et al., 2013) with no major impairment of midbrain neurons function exhibited by the *Cdnf*$^{-/-}$ mice, could represent a phenotype reminiscent of early, pre-motor symptomatic PD. Interestingly alpha-synuclein has been shown to accumulate in the colonic submucosa in early untreated PD (Shannon et al., 2012; Beach et al., 2016; Fenyi et al., 2019); moreover, PD is not associated with loss of myenteric neurons and PD-related GI dysmotility is considered to be more likely due to damage in the submucosal plexus (Annerino et al., 2012).

Even though the ENS was highly affected by the deletion of CDNF, the number of dopaminergic neurons in the SN, the densities of their striatal projections, and the striatal DA concentrations were similar in *Cdnf*$^{-/-}$ and *Cdnf*$^{+/+}$ mice. Although both CDNF and MANF have been implicated in ER stress, we found no signs of abnormal activation of the UPR in the SN or striata of *Cdnf*$^{-/-}$ mice. Various behavioral tests were used to assess motor and non-motor phenotypes that resemble those seen in PD. We found no difference between genotypes in baseline activity and habituation in a novel environment nor in exploratory, anxiety or depression-like behavior. An increase in D-amphetamine-induced hyperlocomotion, however, was detected in *Cdnf*$^{-/-}$ mice in two different genetic backgrounds, indicating that loss of CDNF leads to changes in the function of brain dopaminergic neurons.

Because D-amphetamine stimulates DA release through DAT, we used cyclic voltammetry to examine DA release and reuptake in striatal brain slices. Electrical stimulation released similar amounts of DA from both *Cdnf*$^{-/-}$ and *Cdnf*$^{+/+}$ dorsal striatal dopaminergic terminals; however, in the 6 month-old animals, the DA reuptake was significantly slower in *Cdnf*$^{-/-}$ mice. This difference disappeared in older mice. Although the mechanisms behind the observed difference are unclear, age-dependent changes in the kinetics of DAT-mediated DA reuptake have been described in earlier studies. One study showed faster DA reuptake kinetics together with higher amounts of DAT in the striatum of 5–6 week-old rats than in 12–13 week-old rats (Volz et al., 2009). Another study described complex alterations in release and reuptake kinetics in young, adult or aged rats with adults having the highest DA release and reuptake (Stamford, 1989). In part, these differences can be explained by age-dependent changes in phosphorylation and glycosylation of DAT (Cruz-Muros et al., 2009).

Importantly, the D-amphetamine-induced DAT-mediated DA efflux was greater in $Cdnf^{-/-}$ mice than in $Cdnf^{+/+}$ mice, which could explain the stronger locomotor activation of $Cdnf^{-/-}$ mice after D-amphetamine administration. Another stimulatory drug, GBR 12909, a DAT-inhibitor that does not reverse DAT-mediated transport was used to test this hypothesis. GBR 12909 stimulated the locomotor activity of both genotypes to a similar extent, suggesting that the difference in D-amphetamine's effects on $Cdnf^{-/-}$ mice depends on altered regulation of the reversal of DAT-mediated transport. Our voltammetry data also revealed that, independently of genotype, in older mice, the D-amphetamine-induced DAT reversal occurred faster than in younger animals and there was also a trend towards higher extracellular DA levels due to DAT-mediated DA release. These observations suggest that during aging, DAT becomes more vulnerable to the D-amphetamine-induced reversal of the direction of DA transport, possibly because DAT becomes more susceptible to phosphorylation through PKCβ (Chen et al., 2009).

The contrast between the much greater phenotypic severities of CDNF-deficiency in the ENS than in the brain is striking. The hypoplasia of neurons that occurs selectively in submucosal but not myenteric neurons with no loss of midbrain dopaminergic neurons in $Cdnf^{-/-}$ mice suggests that CDNF could be required for the development/survival of neurons in the ENS but not in the brain. Compensation by other factors for the absence of CDNF in the brain may occur, as has been shown for numerous rodent knockout models, in which compensatory processes have masked expected neurodegenerative phenotypes (Dawson et al., 2010). MANF, the orthologue of CDNF, is expressed in the developing and adult nigrostriatal system in rodent brain and at low levels in neurons of the submucosal and myenteric ganglia (Lindholm et al., 2008; Wang et al., 2014, Supplemental Fig. 2A). Since MANF expression levels in the nigrostriatal pathway are high, we cannot rule out the possibility that MANF compensates for CDNF depletion. Analysis of adult brain in CDNF-MANF double knockout mice would reveal whether these factors can compensate for one another. The greater sensitivity of enteric than CNS neurons to the absence of CDNF in mice might reflect the severe downregulation of GDNF expression in adult gut because enteric neurons are highly GDNF-dependent (Golden et al., 1999). Alternatively, submucosal enteric neurons might be more dependent on the protective effect of CDNF because they are subject to constitutive mechanical stress from intestinal smooth muscle contractions. Stress in the form of inflammation caused by invasion of bacteria into the intestinal lumen also causes degeneration of enteric neurons which increases as a function of age (Becker et al., 2018). The brain is less exposed to inflammation than the gut because of the protecting blood-brain barrier and the absence of a large constitutive microbiome. There is also reason to believe that the submucosal plexus, which is more sensitive than the myenteric to CDNF-deficiency, is also more subject to stress. The myenteric, but not the submucosal plexus is protected by a blood-tissue barrier that is analogous to the blood-brain barrier (Gershon and Bursztajn, 1978).

This is the first study to analyze the function of endogenous CDNF in mammals. The ENS and brain dopaminergic phenotypes in $Cdnf^{-/-}$ mice that we have discovered reveal novel *in vivo* actions of CDNF. We also report, for the first time, that CDNF is critical for the development/maintenance of enteric submucosal neurons; moreover, in the aging brain,

CDNF plays a role in dopaminergic function through the regulation of DAT function in striatal dopaminergic axon terminals.

Supplementary Material

Refer to Web version on PubMed Central for supplementary material.

Acknowledgements

References

Airavaara M, Mijatovic J, Vihavainen T, Piepponen TP, Saarma M, Ahtee L, 2006. In heterozygous GDNF knockout mice the response of striatal dopaminergic system to acute morphine is altered. Synapse 59, 321–329. 10.1002/syn.20245. [PubMed: 16437537]

Airavaara M, Harvey BK, Voutilainen MH, Shen H, Chou J, Lindholm P, Lindahl M, Tuominen RK, Saarma M, Hoffer B, et al. , 2012. CDNF protects the nigrostriatal dopamine system and promotes recovery after MPTP treatment in mice. Cell Transplant. 21, 1213–1223. 10.3727/096368911X600948. [PubMed: 21943517]

Annerino DM, Arshad S, Taylor GM, Adler CH, Beach TG, Greene JC, 2012. Parkinson's disease is not associated with gastrointestinal myenteric ganglion neuron loss. Acta Neuropathol. 124 (5), 665–680. 10.1007/s00401-012-1040-2. [PubMed: 22941241]

Apostolou A, Shen Y, Liang Y, Luo J, Fang S, 2008. Armet, a UPR-upregulated protein, inhibits cell proliferation and ER stress-induced cell death. Exp. Cell Res 314, 2454–2467. 10.1016/j.yexcr.2008.05.001. [PubMed: 18561914]

Bai M, Vozdek R, Hnizda A, Jiang C, Wang B, Kuchar L, Li T, Zhang Y, Wood C, Feng L, et al. , 2018. Conserved roles of C. elegans and human MANFs in sulfatide binding and cytoprotection. Nat. Commun 9, 897. 10.1038/s41467-018-03355-0. [PubMed: 29497057]

Beach TG, Corbille AG, Letournel F, Kordower JH, Kremer T, Munoz DG, Intorcia A, Hentz J, Adler CH, Sue LI, Walker J, Serrano G, Derkinderen P, 2016. Multicenter assessment of Immunohistochemical methods for pathological alpha-synuclein in sigmoid colon of autopsied Parkinson's disease and control subjects. J. Park. Dis 6 (4), 761–770.

Becker L, Nguyen L, Gill J, Kulkarni S, Pasricha PJ, Habtezion A, 2018. Age-dependent shift in macrophage polarisation causes inflammation-mediated degeneration of enteric nervous system. Gut 67 (5), 827–836. 10.1136/gutjnl-2016-312940. [PubMed: 28228489]

Bian GL, Wei LC, Shi M, Wang YQ, Cao R, Chen LW, 2007. Fluoro-jade C can specifically stain the degenerative neurons in the substantia nigra of the 1-methyl-4-phenyl-1,2,3,6-tetrahydropyridine-treated C57BL/6 mice. Brain Res. 1150, 55–61. 10.1016/j.brainres.2007.02.078. [PubMed: 17397812]

Braak H, de Vos RA, Bohl J, Del Tredici K, 2006. Gastric alpha-synuclein immunoreactive inclusions in Meissner's and Auerbach's plexuses in cases staged for Parkinson's disease-related brain pathology. Neurosci. Lett 396, 67–72. 10.1016/j.neulet.2005.11.012. [PubMed: 16330147]

Chalazonitis A, Rao M, 2018. Enteric nervous system manifestations in neurodegenerative disease. Brain Res. 1693, 207–213. 10.1016/j.brainres.2018.01.011. [PubMed: 29360466]

Chalazonitis A, Pham TD, Li Z, Roman D, Guha U, Gomes W, Kan L, Kessler JA, Gershon MD, 2008. Bone morphogenetic protein regulation of enteric neuronal phenotypic diversity: relationship to timing of cell cycle exit. J. Comp. Neurol 509, 474–492. 10.1002/cne.21770. [PubMed: 18537141]

Chalazonitis A, Lindholm P, Gershon MD, 2010. The cerebral dopamine neurotrophic factor (CDNF) selectively promotes acquisition of an enteric dopaminergic neuronal phenotype. In: 40th Annual Meeting of the Society for Neuroscience, pp. 79 Vol. Abstract number 232.19, San Diego, CA.

Chalazonitis A, Tang AA, Shang Y, Pham TD, Hsieh I, Setlik W, Gershon MD, Huang EJ, 2011. Homeodomain interacting protein kinase 2 regulates postnatal development of enteric dopaminergic neurons and glia via BMP signaling. J. Neurosci 31, 13746–13757. 10.1523/JNEUROSCI.1078-11.2011. [PubMed: 21957238]

Chalazonitis A, Gershon MD, Greene LA, 2012. Cell death and the developing enteric nervous system. Neurochem. Int 61, 839–847. 10.1016/j.neuint.2012.01.028. [PubMed: 22342822]

Chalazonitis A, Li Z, Pham TD, Lindahl M, Lindholm-Pulkkila P, Saarma M, Gershon MD, 2013. Enteric neural crest-derived precursors express FoxA2 and the the cerebral dopamine neurotrophic factor (CDNF), which is essential for enteric dopaminergic neuronal development/survival and the maintenance of gastrointestinal motility. In: 43rd Annual Meeting of the Society for Neuroscience. 317. pp. 04 San Diego, CA: Abstract number.

Chen R, Furman CA, Zhang M, Kim MN, Gereau RWT, Leitges M, Gnegy ME, 2009. Protein kinase Cbeta is a critical regulator of dopamine transporter trafficking and regulates the behavioral response to amphetamine in mice. J. Pharmacol. Exp. Ther 328, 912–920. 10.1124/jpet.108.147959. [PubMed: 19098163]

Choi JM, Hong JH, Chae MJ, Ngyuen PH, Kang HS, Ma HI, Kim YJ, 2011. Analysis of mutations and the association between polymorphisms in the cerebral dopamine neurotrophic factor (CDNF) gene and Parkinson disease. Neurosci. Lett 493, 97–101. 10.1016/j.neulet.2011.02.013. [PubMed: 21320571]

Cruz-Muros I, Afonso-Oramas D, Abreu P, Perez-Delgado MM, Rodriguez M, Gonzalez-Hernandez T, 2009. Aging effects on the dopamine transporter expression and compensatory mechanisms. Neurobiol. Aging 30, 973–986. 10.1016/j.neurobiolaging.2007.09.009. [PubMed: 17976862]

Danilova T, Galli E, Pakarinen E, Palm E, Lindholm P, Saarma M, Lindahl M, 2019. Mesencephalic astrocyte-derived neurotrophic factor (MANF) is highly expressed in mouse tissues with metabolic function. Front. Endocrinol 10.3389/fendo.2019.00765.06. 11.

Dawson TM, Ko HS, Dawson VL, 2010. Genetic animal models of Parkinson's disease. Neuron 66, 646–661. 10.1016/j.neuron.2010.04.034. [PubMed: 20547124]

Ehara A, Ueda S, 2009. Application of Fluoro-jade C in acute and chronic neurodegeneration models: utilities and staining differences. Acta Histochem. Cytochem 42, 171–179. 10.1267/ahc.09018. [PubMed: 20126570]

Eskelinen EL, Reggiori F, Baba M, Kovacs AL, Seglen PO, 2011. Seeing is believing: the impact of electron microscopy on autophagy research. Autophagy 7, 935–956. 10.4161/auto.7.9.15760. [PubMed: 21566462]

Fenyi A, Leclair-Visonneau L, Clairembault T, Coron E, Neunlist M, Melki R, Derkinderen P, Bousset L, 2019. Detection of alpha-synuclein aggregates in gastrointestinal biopsies by protein misfolding cyclic amplification. Neurobiol. Dis 129, 38–43. [PubMed: 31078683]

Fleckenstein AE, Volz TJ, Riddle EL, Gibb JW, Hanson GR, 2007. New insights into the mechanism of action of amphetamines. Annu. Rev. Pharmacol. Toxicol 47, 681–698. 10.1146/annurev.pharmtox.47.120505.105140. [PubMed: 17209801]

Garea-Rodriguez E, Eesmaa A, Lindholm P, Schlumbohm C, Konig J, Meller B, Krieglstein K, Helms G, Saarma M, Fuchs E, 2016. Comparative analysis of the effects of Neurotrophic factors CDNF and GDNF in a nonhuman primate model of Parkinson's disease. PLoS One 11, e0149776. 10.1371/journal.pone.0149776. [PubMed: 26901822]

Gershon MD, Bursztajn S, 1978. Properties of the enteric nervous system: limitation of access of intravascular macromolecules to the myenteric plexus and muscularis externa. J. Comp. Neurol 180, 467–488. 10.1002/cne.901800305. [PubMed: 659670]

Gianino S, Grider JR, Cresswell J, Enomoto H, Heuckeroth RO, 2003. GDNF availability determines enteric neuron number by controlling precursor proliferation. Development 130, 2187–2198. 10.1242/dev.00433. [PubMed: 12668632]

Glembotski CC, Thuerauf DJ, Huang C, Vekich JA, Gottlieb RA, Doroudgar S, 2012. Mesencephalic astrocyte-derived neurotrophic factor protects the heart from ischemic damage and is selectively secreted upon sarco/endoplasmic reticulum calcium depletion. J. Biol. Chem 287, 25893–25904. 10.1074/jbc.M112.356345. [PubMed: 22637475]

Golden JP, DeMaro JA, Osborne PA, Milbrandt J, Johnson EM Jr., 1999. Expression of neurturin, GDNF, and GDNF family-receptor mRNA in the developing and mature mouse. Exp. Neurol 158, 504–528. 10.1006/exnr.1999.7127. [PubMed: 10415156]

Henderson MJ, Richie CT, Airavaara M, Wang Y, Harvey BK, 2013. Mesencephalic astrocyte-derived neurotrophic factor (MANF) secretion and cell surface binding are modulated by KDEL receptors. J. Biol. Chem 288, 4209–4225. 10.1074/jbc.M112.400648. [PubMed: 23255601]

Hoang T, Choi D-K, Nagai M, Wu D-C, Nagata T, Prou D, Wilson GL, Vila M, Jackson-Lewis V, Dawson V, Dawson TM, Chesselet M-F, Przedborski S, 2009. Neuronal NOS and cyclooxygenase-2 contribute to DNA damage in a mouse model of Parkinson's disease. Free Radic. Biol. Med 47, 1049–1056. 10.1016/j.freeradbiomed.2009.07.013. [PubMed: 19616617]

Holubec H, Payne CM, Bernstein H, Dvorakova K, Bernstein C, Waltmire CN, Warneke JA, Garewal H, 2005. Assessment of apoptosis by immunohistochemical markers compared to cellular morphology in ex vivo-stressed colonic mucosa. J. Histochem. Cytochem 53, 229–235. 10.1369/jhc.4A6386.2005. [PubMed: 15684335]

Hoozemans JJ, Scheper W, 2012. Endoplasmic reticulum: the unfolded protein response is tangled in neurodegeneration. Int. J. Biochem. Cell Biol 44, 1295–1298. 10.1016/j.biocel.2012.04.023. [PubMed: 22564438]

House NCM, Koch MR, Freudenreich CH, 2014. Chromatin modifications and DNA repair: beyond double-strand breaks. Front. Genet 10.3389/fgene.2014.00296. 05 9.

Hung KC, Huang HJ, Lin MW, Lei YP, Lin AM, 2014. Roles of autophagy in MPP +-induced neurotoxicity in vivo: the involvement of mitochondria and alpha-synuclein aggregation. PLoS One 9, e91074. 10.1371/journal.pone.0091074. [PubMed: 24646838]

Huttunen HJ, Saarma M, 2019. CDNF protein therapy in Parkinson's disease. Cell. Tranplant 28 (4), 349–366. 10.1177/0963689719840290.

Jackson-Lewis V, Jakowec M, Burke RE, Przedborski S, 1995. Time course and morphology of dopmimergic neuronal death caused by the neurotoxin1-methyl-4-phenyl 1,2,3,6 tetrahydropyridine. Neurodegeneration 4, 257–269. [PubMed: 8581558]

Jiang Y, Liu M, Gershon MD, 2003. Netrins and DCC in the guidance of migrating neural crest-derived cells in the developing bowel and pancreas. Dev. Biol 258, 364–384. 10.1016/s0012-1606(03)00136-2. [PubMed: 12798294]

Kemppainen S, Lindholm P, Galli E, Lahtinen HM, Koivisto H, Hamalainen E, Saarma M, Tanila H, 2015. Cerebral dopamine neurotrophic factor improves long-term memory in APP/PS1 transgenic mice modeling Alzheimer's disease as well as in wild-type mice. Behav. Brain Res. 291, 1–11. 10.1016/j.bbr.2015.05.002. [PubMed: 25975173]

King PH, Redden D, Palmgren JS, Nabors LB, Lennon VA, 1999. Hu antigen specificities of ANNA-1 autoantibodies in paraneoplastic neurological disease. J. Autoimmun 13, 435–443. 10.1006/jaut.1999.0337. [PubMed: 10585760]

Kumar A, Kopra J, Varendi K, Porokuokka LL, Panhelainen A, Kuure S, Marshall P, Karalija N, Harma MA, Vilenius C, et al. , 2016. Correction: GDNF overexpression from the native locus reveals its role in the Nigrostriatal dopaminergic system function. PLoS Genet. 12, e1005808. 10.1371/journal.pgen.1005808. [PubMed: 26752407]

Kupsky WJ, Grimes MM, Sweeting J, Bertsch R, Cote LJ, 1987. Parkinson's disease and megacolon: concentric hyaline inclusions (Lewy bodies) in enteric ganglion cells. Neurology 37, 1253–1255. 10.1212/wnl.37.7.1253. [PubMed: 3037441]

Lebouvier T, Neunlist M, Bruley, des, Varannes S, Coron E, Drouard A, N'Guyen JM, Chaumette T, Tasselli M, Paillusson S, Flamand M, Galmiche J-P, Damier P, Derkinderen P, 2010. Colonic

biopsies to assess the neuropathology of Parkinson's disease and its relationship with symptoms. PLoS One 5 (9). 10.1371/journal.pone.0012728.

Li ZS, Pham TD, Tamir H, Chen JJ, Gershon MD, 2004. Enteric dopaminergic neurons: definition, developmental lineage and effects of extrinsic denervation. J. Neurosci 24, 1330–1339. 10.1523/JNEUROSCI.3982-03.2004. [PubMed: 14960604]

Li Z, Chalazonitis A, Huang YY, Mann JJ, Margolis KG, Yang QM, Kim DO, Cote F, Mallet J, Gershon MD, 2011. Essential roles of enteric neuronal serotonin in gastrointestinal motility and the development/survival of enteric dopaminergic neurons. J. Neurosci 31, 8998–9009. [PubMed: 21677183]

Lindahl M, Danilova T, Palm E, Lindholm P, Voikar V, Hakonen E, Ustinov J, Andressoo JO, Harvey BK, Otonkoski T, et al. , 2014. MANF is indispensable for the proliferation and survival of pancreatic beta cells. Cell Rep. 7, 366–375. 10.1016/j.celrep.2014.03.023. [PubMed: 24726366]

Lindahl M, Saarma M, Lindholm P, 2017. Unconventional neurotrophic factors CDNF and MANF: structure, physiological functions and therapeutic potential. Neurobiol. Dis 97, 90–102. 10.1016/j.nbd.2016.07.009. [PubMed: 27425895]

Lindholm D, Wootz H, Korhonen L, 2006. ER stress and neurodegenerative diseases. Cell Death Differ. 13, 385–392. 10.1038/sj.cdd.4401778. [PubMed: 16397584]

Lindholm P, Voutilainen MH, Lauren J, Peranen J, Leppanen VM, Andressoo JO, Lindahl M, Janhunen S, Kalkkinen N, Timmusk T, et al. , 2007. Novel neurotrophic factor CDNF protects and rescues midbrain dopamine neurons in vivo. Nature 448, 73–77. 10.1038/nature05957. [PubMed: 17611540]

Lindholm P, Peranen J, Andressoo JO, Kalkkinen N, Kokaia Z, Lindvall O, Timmusk T, Saarma M, 2008. MANF is widely expressed in mammalian tissues and differently regulated after ischemic and epileptic insults in rodent brain. Mol. Cell. Neurosci 39, 356–371. 10.1016/j.mcn.2008.07.016. [PubMed: 18718866]

Liu MT, Kuan YH, Wang J, Hen R, Gershon MD, 2009. 5-HT4 receptor-mediated neuroprotection and neurogenesis in the enteric nervous system of adult mice. J. Neurosci 29, 9683–9699. 10.1523/JNEUROSCI.1145-09.2009. [PubMed: 19657021]

Lu C, Zhu F, Cho Y-Y, Tang F, Zykova T, Ma W-Y, Bode AM, Dong Z, 2006. Cell apoptosis: requirement of H2A.X in DNA ladder formation, but not for the activation of Caspase-3. Mol. Cell 23, 121–132. 10.1016/j.molcel.2006.05.023. [PubMed: 16818236]

Lynch-Day MA, Mao K, Wang K, Zhao M, Klionsky DJ, 2012. The role of autophagy in Parkinson's disease. Cold Spring Harbor Perspect. Med 2, a009357. 10.1101/cshperspect.a009357.

Margolis KG, Li Z, Stevanovic K, Saurman V, Israelyan N, Anderson GM, et al. , 2016. Serotonin transporter variant drives preventable gastrointestinal abnormalities in development and function. J. Clin. Invest 126 (6), 2221–2235. 10.1172/JCI84877. [PubMed: 27111230]

Martinez BA, Petersen DA, Gaeta AL, Stanley SP, Caldwell GA, Caldwell KA, 2017. Dysregulation of the mitochondrial unfolded protein response induces non-apoptotic dopaminergic neurodegeneration in *C. elegans* models of Parkinson's disease. J. Neurosci 37 (46), 11085–11100. 10.1523/JNEUROSCI.1294-17.2017. [PubMed: 29030433]

Matlik K, Yu LY, Eesmaa A, Hellman M, Lindholm P, Peranen J, Galli E, Anttila J, Saarma M, Permi P, et al. , 2015. Role of two sequence motifs of mesencephalic astrocyte-derived neurotrophic factor in its survival-promoting activity. Cell Death Dis. 6, e2032. 10.1038/cddis.2015.371. [PubMed: 26720341]

McKeown SJ, Chow CW, Young HM, 2001. Development of the submucous plexus in the large intestine of the mouse. Cell Tissue Res. 303, 301–305. 10.1007/s004410000303. [PubMed: 11291776]

Michel PP, Hirsch EC, Hunot S, 2016. Understanding dopaminergic cell death pathways in Parkinson disease. Neuron 90, 675–691. 10.1016/j.neuron.2016.03.038. [PubMed: 27196972]

Mijatovic J, Airavaara M, Planken A, Auvinen P, Raasmaja A, Piepponen TP, Costantini F, Ahtee L, Saarma M, 2007. Constitutive ret activity in knock-in multiple endocrine neoplasia type B mice induces profound elevation of brain dopamine concentration via enhanced synthesis and increases the number of TH-positive cells in the substantia nigra. J. Neurosci 27, 4799–4809. 10.1523/JNEUROSCI.5647-06.2007. [PubMed: 17475787]

Mizobuchi N, Hoseki J, Kubota H, Toyokuni S, Nozaki J, Naitoh M, Koizumi A, Nagata K, 2007. ARMET is a soluble ER protein induced by the unfolded protein response via ERSE-II element. Cell Struct. Funct 32, 41–50. [PubMed: 17507765]

Mongardi Fantaguzzi C, Thacker M, Chiocchetti R, Furness JB, 2009. Identification of neuron types in the submucosal ganglia of the mouse ileum. Cell Tissue Res. 336, 179–189. 10.1007/s00441-009-0773-2. [PubMed: 19326148]

Payette RF, Bennett GS, Gershon MD, 1984. Neurofilament expression in vagal neural crest-derived precursors of enteric neurons. Dev. Biol 105, 273–287. 10.1016/0012-1606(84)90285-9. [PubMed: 6383899]

Penttinen AM, Suleymanova I, Albert K, Anttila J, Voutilainen MH, Airavaara M, 2016. Characterization of a new low-dose 6-hydroxydopamine model of Parkinson's disease in rat. J. Neurosci. Res 94, 318–328. 10.1002/jnr.23708. [PubMed: 26762168]

Petrova P, Raibekas A, Pevsner J, Vigo N, Anafi M, Moore MK, Peaire AE, Shridhar V, Smith DI, Kelly J, et al. , 2003. MANF: a new mesencephalic, astrocyte-derived neurotrophic factor with selectivity for dopaminergic neurons. J. Mol. Neurosci 20, 173–188. [PubMed: 12794311]

Pfeiffer RF, 2003. Gastrointestinal dysfunction in Parkinson's disease. Lancet Neurol. 2, 107–116. [PubMed: 12849267]

Pham TD, Gershon MD, Rothman TP, 1991. Time of origin of neurons in the murine enteric nervous system: sequence in relation to phenotype. J. Comp. Neurol 314, 789–798. 10.1002/cne.903140411. [PubMed: 1816276]

Rao M, Gershon MD, 2016. The bowel and beyond: the enteric nervous system in neurological disorders. Nat. Rev. Gastroenterol. Hepatol 13, 517–528. 10.1038/nrgastro.2016.107. [PubMed: 27435372]

Rao M, Nelms BD, Dong L, Salinas-Rios V, Rutlin M, Gershon MD, Corfas G, 2015. Enteric glia express proteolipid protein 1 and are a transcriptionally unique population of glia in the mammalian nervous system. Glia. 10.1002/glia.22876.

Ratcliffe EM, D'Autreaux F, Gershon MD, 2008. Laminin terminates the Netrin/DCC mediated attraction of vagal sensory axons. Dev. Neurobiol 68, 960–971. 10.1002/dneu.20634. [PubMed: 18418846]

Ren X, Zhang T, Gong X, Hu G, Ding W, Wang X, 2013. AAV2-mediated striatum delivery of human CDNF prevents the deterioration of midbrain dopamine neurons in a 6-hydroxydopamine induced parkinsonian rat model. Exp. Neurol 248, 148–156. 10.1016/j.expneurol.2013.06.002. [PubMed: 23764500]

Rogakou EP, Nieves-Neira W, Boon C, Pommier Y, Bonner WM, 2000. Initiation of DNA fragmentation during apoptosis induces phosphorylation of H2AX histone at serine 139. J. Biol. Chem 275, 9390–9395. 10.1074/jbc.275.13.9390. [PubMed: 10734083]

Schmued LC, Albertson C, Slikker W Jr., 1997. Fluoro-jade: a novel fluorochrome for the sensitive and reliable histochemical localization of neuronal degeneration. Brain Res. 751, 37–46. 10.1016/s0006-8993(96)01387-x. [PubMed: 9098566]

Shannon KM, Keshavarzian A, Mutlu E, Dodiya HB, Dalan D, Jaglin JA, Dower JH, 2012. Alpha-synuclein in colonic submucosa in early untreated Parkinson's disease. Mov. Disord 27 (6), 709–715. 10.1002/mds.23838. [PubMed: 21766334]

Singaram C, Ashraf W, Gaumnitz EA, Torbey C, Sengupta A, Pfeiffer R, Quigley EM, 1995. Dopaminergic defect of enteric nervous system in Parkinson's disease patients with chronic constipation. Lancet 346, 861–864. 10.1016/s0140-6736(95)92707-7. [PubMed: 7564669]

Stamford JA, 1989. Development and ageing of the rat nigrostriatal dopamine system studied with fast cyclic voltammetry. J. Neurochem 52, 1582–1589. 10.1111/j.1471-4159.1989.tb09212.x. [PubMed: 2709014]

Taylor TN, Greene JG, Miller GW, 2010. Behavioral phenotyping of mouse models of Parkinson's disease. Behav. Brain Res 211, 1–10. 10.1016/j.bbr.2010.03.004. [PubMed: 20211655]

Tseng KY, Danilova T, Domanskyi A, Saarma M, Lindahl M, Airavaara M, 2017. MANF is essential for neurite extension and neuronal migration in the developing cortex. eNeuro 4. 10.1523/ENEURO.0214-17.2017.

van der Weiden L, Adams DJ, Harris LW, Tannahill D, Arends MJ, Bradley A, 2005. Null and conditional semaphorin 3B alleles using a flexible puroDelta tk loxP/Frt vector. Genesis 41 (4), 171–178. 10.1002/gene.20111. [PubMed: 15789413]

Volz TJ, Farnsworth SJ, Rowley SD, Hanson GR, Fleckenstein AE, 2009. Age-dependent differences in dopamine transporter and vesicular monoamine transporter-2 function and their implications for methamphetamine neurotoxicity. Synapse 63, 147–151. 10.1002/syn.20580. [PubMed: 19021208]

Voutilainen MH, Back S, Porsti E, Toppinen L, Lindgren L, Lindholm P, Peranen J, Saarma M, Tuominen RK, 2009. Mesencephalic astrocyte-derived neurotrophic factor is neurorestorative in rat model of Parkinson's disease. J. Neurosci 29, 9651–9659. 10.1523/JNEUROSCI.0833-09.2009. [PubMed: 19641128]

Voutilainen MH, Back S, Peranen J, Lindholm P, Raasmaja A, Mannisto PT, Saarma M, Tuominen RK, 2011. Chronic infusion of CDNF prevents 6-OHDA-induced deficits in a rat model of Parkinson's disease. Exp. Neurol 228, 99–108. 10.1016/j.expneurol.2010.12.013. [PubMed: 21185834]

Voutilainen MH, De Lorenzo F, Stepanova P, Back S, Yu LY, Lindholm P, Porsti E, Saarma M, Mannisto PT, Tuominen RK, 2017. Evidence for an additive Neurorestorative effect of simultaneously administered CDNF and GDNF in Hemiparkinsonian rats: implications for different mechanism of action. eNeuro 4. 10.1523/ENEURO.0117-16.2017.

Wang M, Kaufman RJ, 2016. Protein misfolding in the endoplasmic reticulum as a conduit to human disease. Nature 529, 326–335. 10.1038/nature17041. [PubMed: 26791723]

Wang H, Ke Z, Alimov A, Xu M, Frank JA, Fang S, Luo J, 2014. Spatiotemporal expression of MANF in the developing rat brain. PLoS One 9, e90433. 10.1371/journal.pone.0090433. [PubMed: 24587361]

Wilson AJ, Holson E, Wagner F, Zhang YL, Fass DM, Haggarty SJ, Bhaskara S, Hiebert SW, Schreiber SL, Khabele D, 2011. The DNA damage mark pH2AX differentiates the cytotoxic effects of small molecule HDAC inhibitors in ovarian cancer cells. Cancer. Biol. Ther 12, 484–493. 10.4161/cbt.12.6.15956. [PubMed: 21738006]

Yates JW, Meij JT, Sullivan JR, Richtand NM, Yu L, 2007. Bimodal effect of amphetamine on motor behaviors in C57BL/6 mice. Neurosci. Lett 427, 66–70. 10.1016/j.neulet.2007.09.011. [PubMed: 17920769]

Zhang G-L, Wang L-H, Liu X-Y, Zhang Y-X, Hu M-Y, Liu L, Fang Y-Y, Mu Y, Zhao Y, Huang S-H, Liu T, Wang X-J, 2018. Cerebral dopamine Neurotrophic factor (CDNF) has Neuroprotective effects against cerebral ischemia that may occur through the endoplasmic reticulum stress pathway. Int. J Mol Scl 19, 1905–1917. 10.3390/ijms19071905.

Zhou W, Chang L, Fang Y, Du Z, Li Y, Song Y, Hao F, Lv L, Wu Y, 2016. Cerebral dopamine neurotrophic factor alleviates Abeta25–35-induced endoplasmic reticulum stress and early synaptotoxicity in rat hippocampal cells. Neurosci. Lett 633, 40–46. 10.1016/j.neulet.2016.09.008. [PubMed: 27616705]
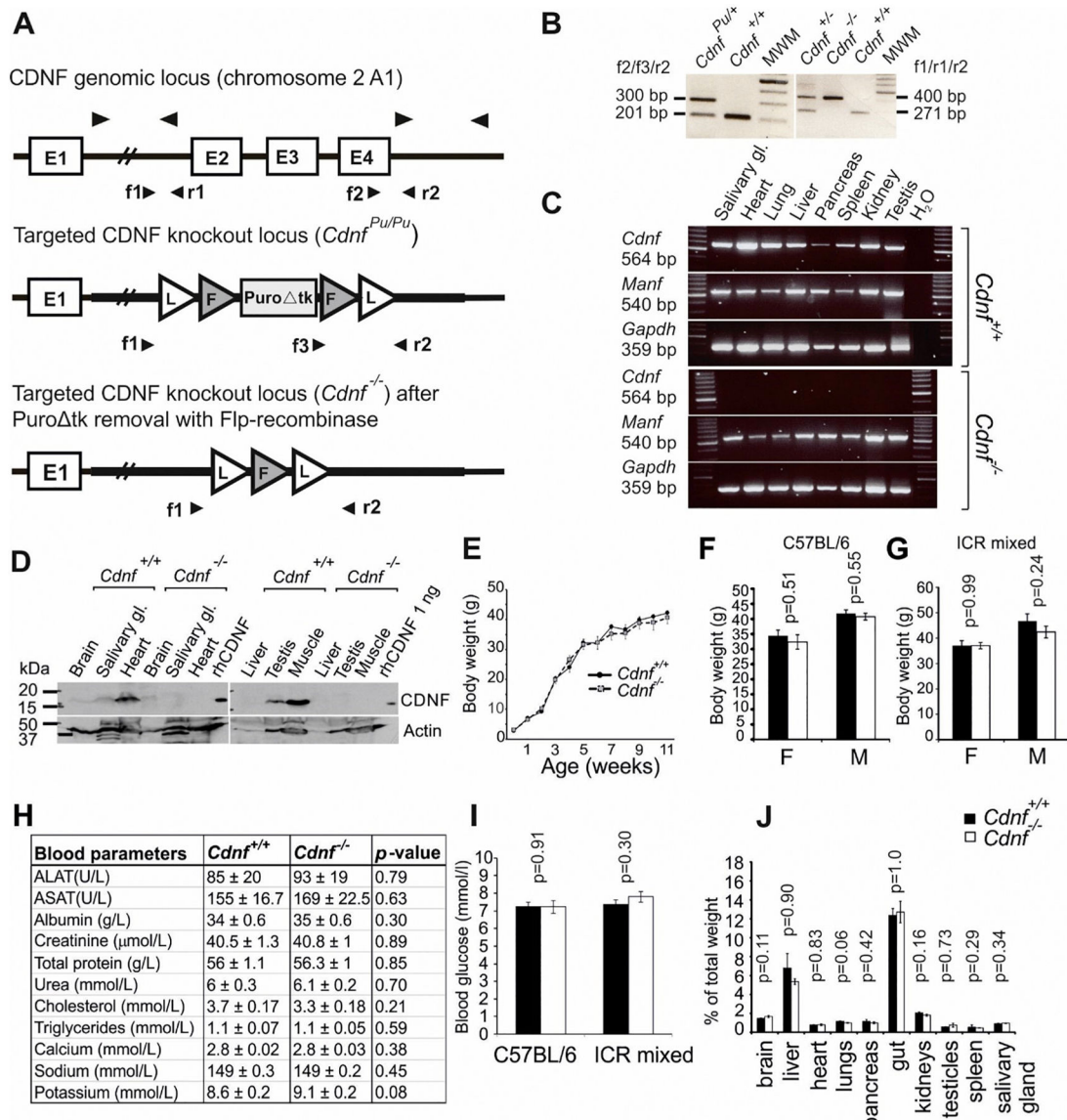
Fig. 1.
Cdnf knockout mice are viable, fertile and show no obvious gross phenotypes. (**A**)
Schematic illustration of the WT *Cdnf*$^{+/+}$ and targeted *Cdnf*$^{Pu/Pu}$ and *Cdnf*$^{-/-}$ loci.
Arrowheads indicate priming sites used in genotyping by PCR and in RT-PCR. A PGK-
promoter driven puromycin selection cassette (Puro tk), exon (E), Frt (F)-site, LoxP (L)-
site. (**B**). Example of genotyping result. Genotyping of mice was performed by PCR using
primers forward 1 (f1), forward 2 (f2) and forward 3 (f3) and reverse 2 (r2), indicated
by arrowheads in (**A**). Amplified band of 201 bp represents WT *Cdnf*$^{+/+}$, band of 300 bp
represents the targeted *Cdnf*$^{Pu/Pu}$ allele, where puromycin cassette is included (left panel).
In the right panel, amplified band of 400 bp represents the targeted allele from which the
puromycin cassette has been deleted, and the 271 bp band the WT band. MWM; molecular
weight marker. (**C**) RT-PCR analysis for *Cdnf* and *Manf* mRNA expression in tissues from
adult *Cdnf*$^{+/+}$ and *Cdnf*$^{-/-}$ mice. Primers for *Gapdh* were used to normalize mRNA levels

in each sample. (**D**) Western blot analysis of tissue-lysates confirms that CDNF protein is not expressed in tissues of $Cdnf^{-/-}$ mice. Recombinant human CDNF protein (rhCDNF) was used as a positive control and anti-actin antibody for normalization of total protein content. (**E**) Growth curve of $Cdnf^{+/+}$ ($n = 5$) and $Cdnf^{-/-}$ ($n = 5$) littermate male mice. Body weight was measured weekly from postnatal day (P) P3 to 11 weeks of age (two-way RM ANOVA, interaction of genotype and time, $F(11,88) = 1.08$, $p = .387$). Weight of 1 year-old $Cdnf^{+/+}$ and $Cdnf^{-/-}$ female and male mice in (**F**) C57BL/6 background ($n = 6$–14, two-tailed t-test), and (**G**) ICR/C57BL/6 mixed background ($n = 6$, two-tailed t-test, males; Mann Whitney U test). (**H**) Analysis of the indicated components from blood serum of 1 year-old $Cdnf^{+/+}$ ($n = 12$) and $Cdnf^{-/-}$ ($n = 14$) male mice. Differences were analyzed with t-test and calcium content by t-test with Welch's correction. (**I**) *Ad libitum* fed blood glucose levels from 1 year-old $Cdnf^{+/+}$ and $Cdnf^{-/-}$ mice in C57BL/6 background ($n = 19$–20, males; t-test (Welch's correction) and mixed background ($n = 9$–10, males; t-test). (**J**) Organ weights normalized to body weight did not differ between genotypes in 2 year-old (males, $n = 4, 5$) $Cdnf^{+/+}$ and $Cdnf^{-/-}$ mice (t-test; for brain, liver, gut, testicles and spleen, Mann Whitney U test). Mean ± SEM. F, female, M, male.
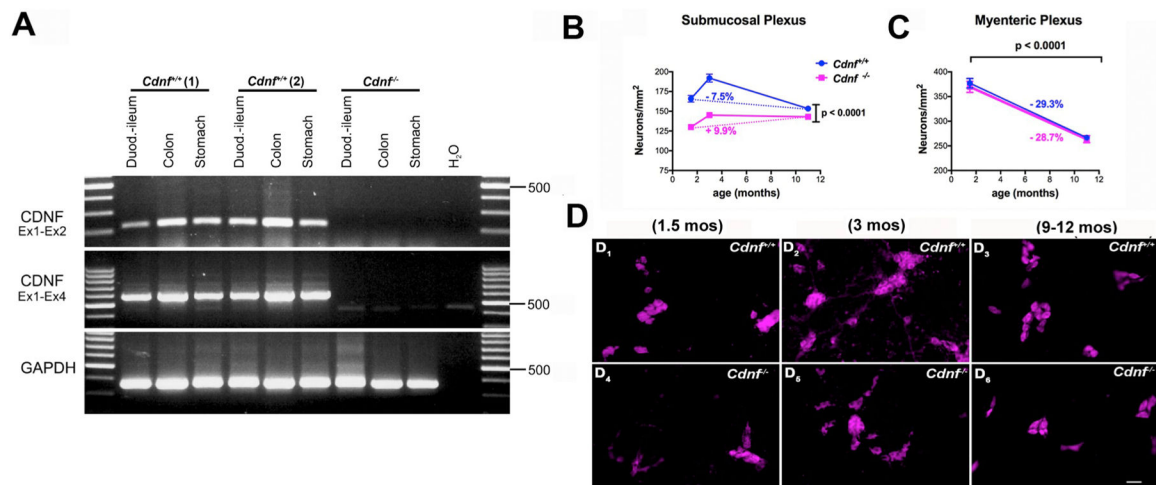
Fig. 2. The degree of selective neuronal hypoplasia is sustained as a function of age in the submucosal plexus of $Cdnf^{-/-}$ mice while in the myenteric plexus the age-dependent decline is similar with no hypoplasia compared to $Cdnf^{+/+}$ mice;

(**A**) Transcripts encoding CDNF are expressed in stomach, intestine and colon of the murine gut at P7 but are absent in $Cdnf^{-/-}$ mice. (**B**) Neuronal densities per mm^2 of plexus in the ileal submucosal plexuses, and (**C**) in the myenteric plexus in $Cdnf^{-/-}$ mice (magenta solid line) and $Cdnf^{+/+}$ mice (blue solid line) are plotted as a function of age. The neuronal densities in the submucosal plexus are significantly lower in $Cdnf^{-/-}$ mice than in $Cdnf^{+/+}$ mice at each age examined; [B] 2 way ANOVA $F(2, 437) = 22.94$. There is however some compensation between 1.5 and 11 month of age in $Cdnf^{-/-}$ mice which does not occur in the $Cdnf^{+/+}$ mice; [C] in contrast in the myenteric plexus the decline as a function of age is similar in $Cdnf^{-/-}$ and in $Cdnf^{+/+}$ mice without compensation between the genotypes. The numbers of animals were 3 $Cdnf^{-/-}$ and 3 $Cdnf^{+/+}$ for 1.5 month-old mice; 6 $Cdnf^{-/-}$ and 6 $Cdnf^{+/+}$ for 3 month-old animals; 7 $Cdnf^{-/-}$ and 7 $Cdnf^{+/+}$ for 9–12 month-old mice; (**D**) Immunocytochemical detection of neurons using antibodies to HuC/D in whole mount laminar preparations of the ileal submucosal plexus in $Cdnf^{+/+}$ (D$_1$-D$_3$) and $Cdnf^{-/-}$ mice (D$_4$-D$_6$) (scale bar, 32 μm).
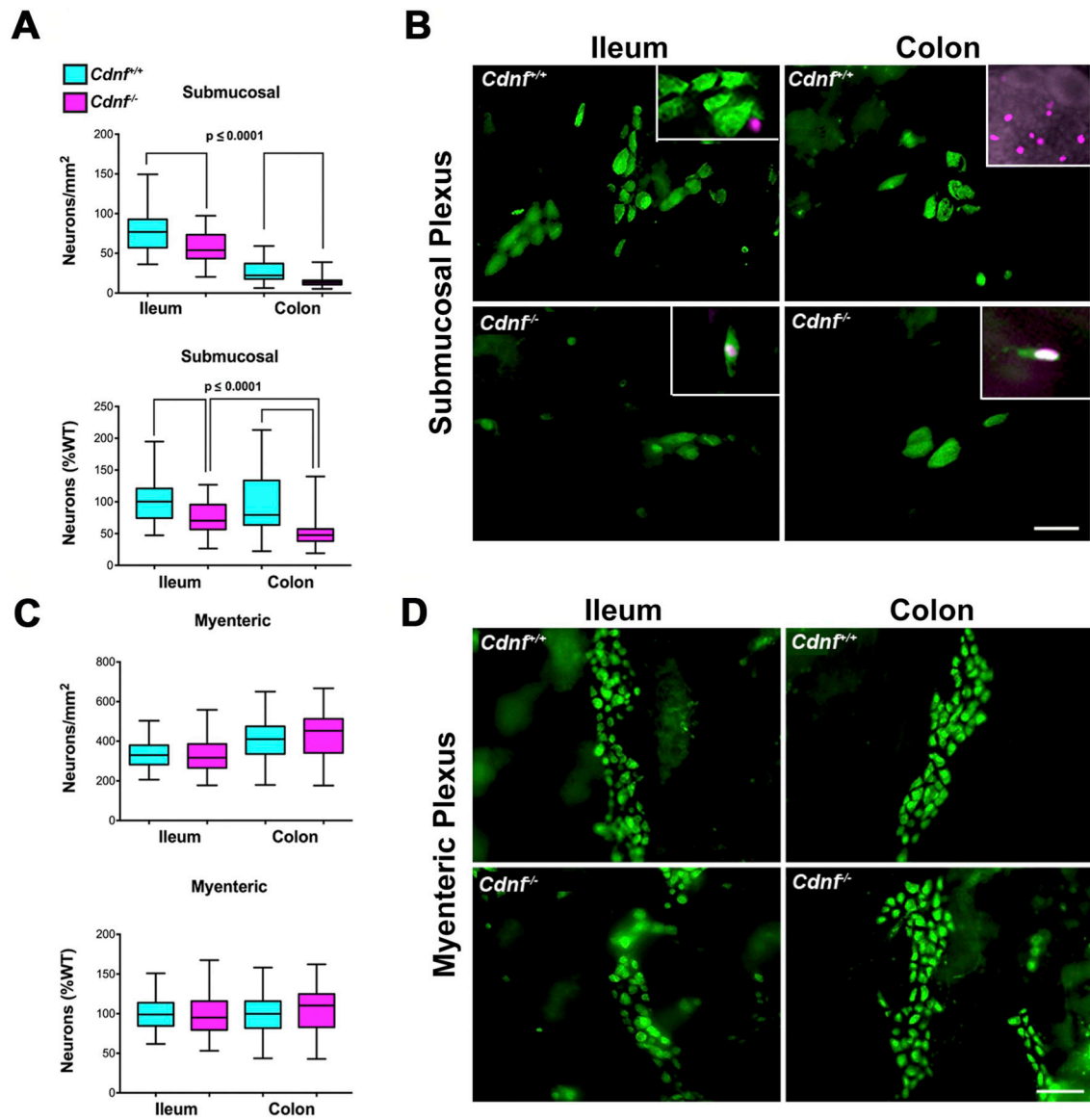
Fig. 3. The selective neuronal hypoplasia in the submucosal plexus of *Cdnf*^{−/−} mice is not the result of increased apoptosis

(**A**) Neuronal densities in the submucosal plexus of 1.5 month-old mice are significantly less both in ileum and colon of *Cdnf*^{−/−} mice ($n = 6$) (magenta,75–91 measurements) than in their *Cdnf*^{+/+} littermates ($n = 4$) (turquoise, 65–82 measurements). Top graph (neurons/mm^2), t-test (with Welch's correction), ileum $t = 5.652$, df = 112.5; colon $t = 8.431$, df = 156. Bottom graph, neurons (% WT); ileum t = 5.652, df = 112.5; colon $t = 7.567$, df = 82.93. (**B**) Immunocytochemical detection of neurons using antibodies to ANNA-1 (green) in optically cleared whole mounts of the ileal and colonic submucosal plexuses in *Cdnf*^{+/+} and *Cdnf*^{−/−} mice (scale bar, 70 μm). Two examples of the very rare apoptotic neurons found in the submucosal plexus in the ileum and colon of *Cdnf*^{−/−} mice, which are co-labeled with ANNA-1 antibodies (green) and the nuclear PH2A.X antibodies (magenta) are shown in the insets of the lower panels. A non-neuronal apoptotic cell is shown (inset left upper panel) in the ileum of a *Cdnf*^{+/+} mouse. In the colon, PH2A.X-immunoreactive

cells are abundant in the epithelium of the mucosa and in lymphoid follicles (inset right upper panel). **(C)** Densities of myenteric neurons differ significantly neither in the ileum nor the colon of juvenile $Cdnf^{-/-}$ mice from those of their $Cdnf^{+/+}$ littermates. Top graph (neurons/mm^2), t-test (Welch's correction), ileum $t = 0.4938$, df = 137.2; colon $t = 1.449$, df = 171. Bottom graph (neuron density %WT), t-test (Welch's correction), ileum $t = 0.4861$ df = 138; colon t = 1.449, df = 171. **(D)** Immunocytochemical detection of neurons using antibodies to ANNA-1 (green) in optically cleared whole mounts of the ileal and colonic myenteric plexuses in $Cdnf^{+/+}$ and $Cdnf^{-/-}$ mice (scale bar, 70 μm).
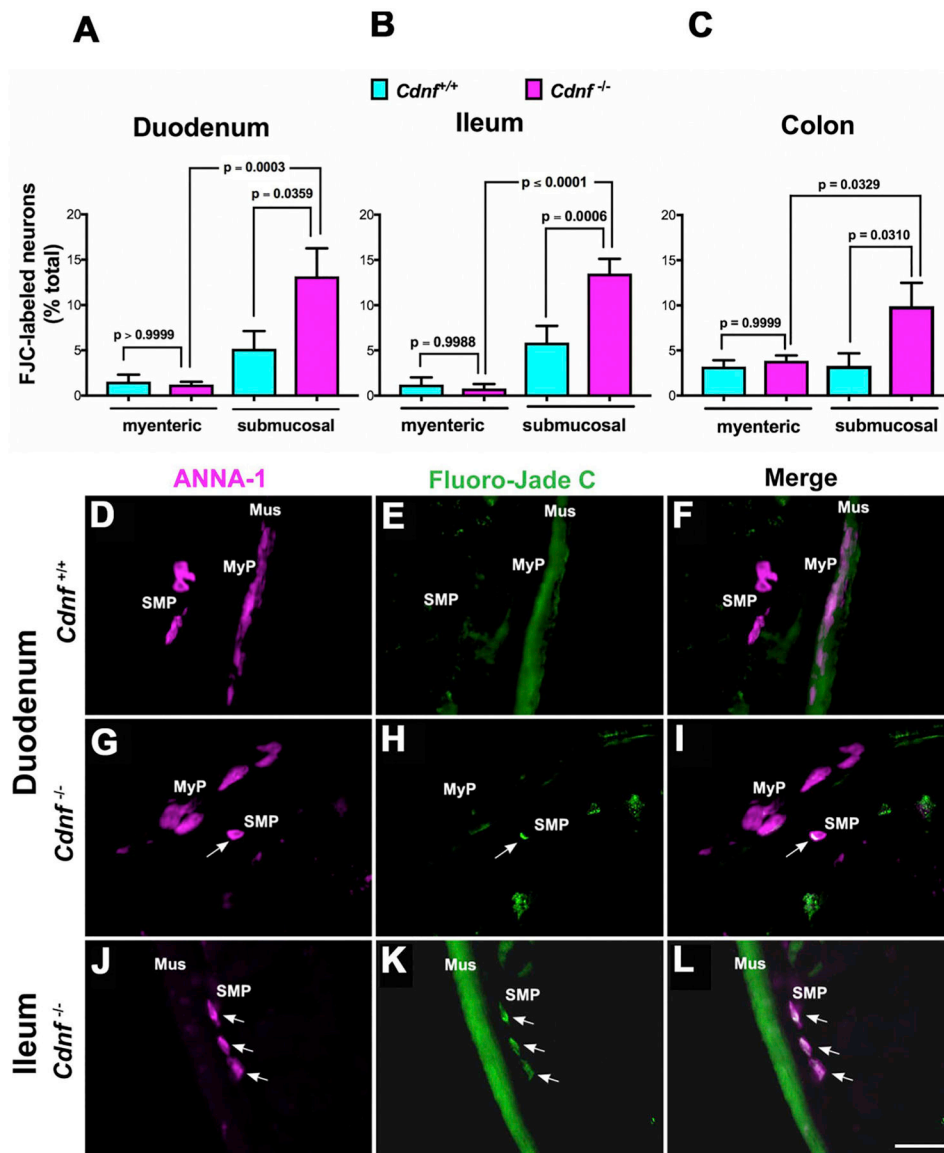
Fig. 4. Neurodegeneration selectively occurs in submucosal neurons of the duodenum, ileum and colon of *Cdnf*$^{-/-}$ mice.

Histochemistry was used with sections cut in a cryostat-microtome to analyze the proportions of neurons that were degenerating in the ENS of 1.5 month-old mice. Neurons were marked with ANNA-1 antibodies (magenta), degeneration with Fluoro-Jade C (FJC; green). The proportion of FJC-labeled neurons in the submucosal plexus of the duodenum (A), ileum (B) and colon (C) of *Cdnf*$^{-/-}$ mice (magenta bars) is significantly greater than that of their *Cdnf*$^{+/+}$ littermates (turquoise bars). In contrast, the proportion of FJC-labeled neurons in the myenteric plexus of the duodenum (A), ileum (B) and colon (C) of *Cdnf*$^{-/-}$ mice does not differ significantly from that of their *Cdnf*$^{+/+}$ littermates. [A, One way Anova, F (3, 34) =8.398 with Sidak's multiple comparisons to compute the *p* values shown in the graph; B, One way Anova, F (3, 50) =21.93 with Sidak's multiple comparisons to compute the p values shown in the graph; C, One way Anova, F (3, 92) =4.357 with Sidak's multiple comparisons to compute the p values shown in the graph]. (D-L) Images of neurons (D,

G, J) with coincident FJC labeling (E, H, K) in the duodenum and ileum of $Cdnf^{+/+}$ (D, E, F) and $Cdnf^{-/-}$ (G-L) mice. Merged images are shown in panels F, I, L. Mus = smooth muscle layer; MyP = myenteric plexus; SMP = submucosal plexus. The arrows point to the locations of FJC-labeled degenerating neurons. The green fluorescence of the muscle layer is due to the non-specific FJC staining of smooth muscle. Scale bar, 35 μm.
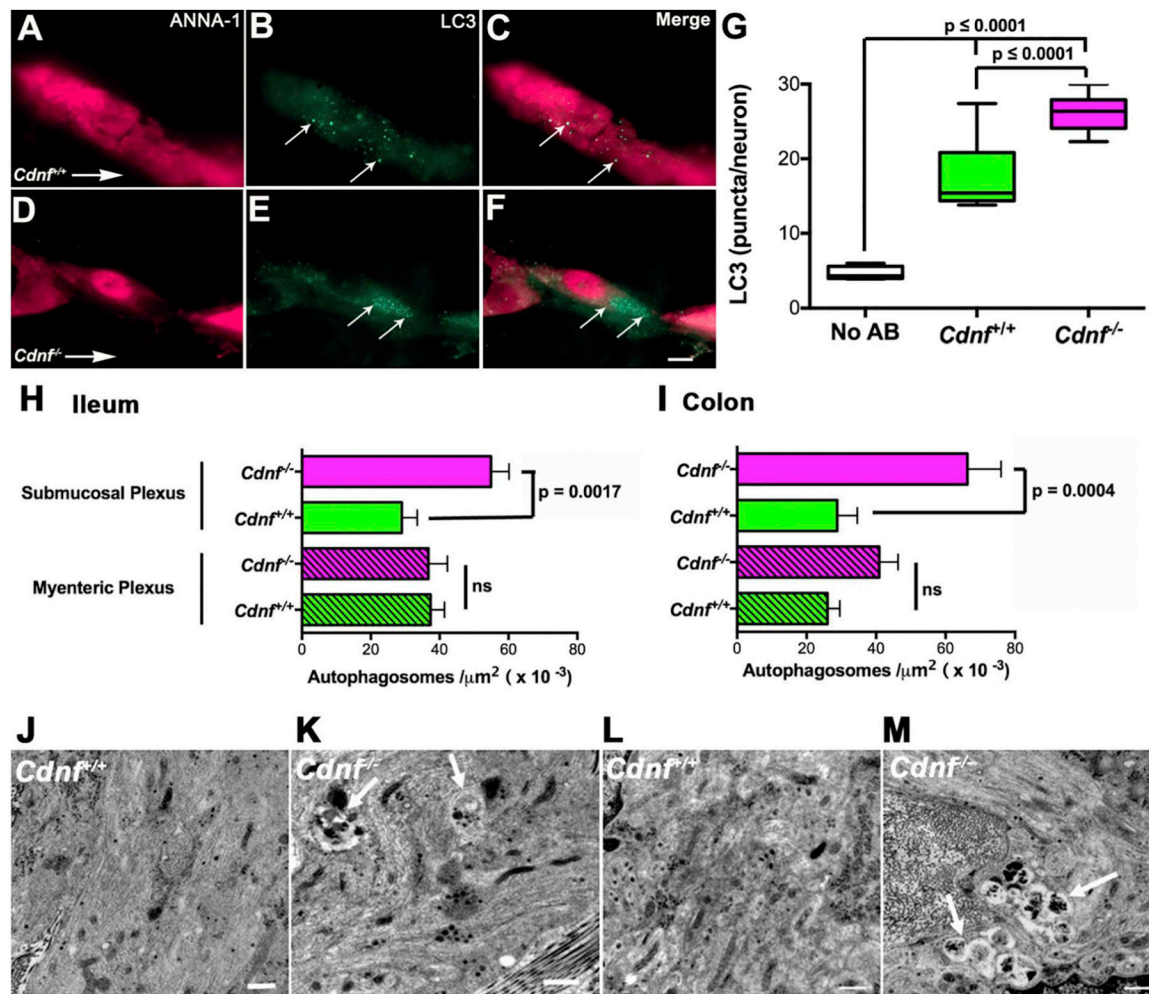
Fig. 5. Density of autophagosomes detected with antibodies to LC3 or electron microscopy is greater in enteric neurons of 11 month-old $Cdnf^{-/-}$ than $Cdnf^{+/+}$ mice.

(**A-F**) Neurons were marked immunocytochemically with antibodies to ANNA-1 (magenta) and autophagic figures were detected as puncta immunostained with antibodies to LC3 (green) in $Cdnf^{+/+}$ (A-C) and $Cdnf^{-/-}$ mice (D-F). The same fields are illustrated in panel A-C and D-F, illuminated to show the fluorescence of ANNA-1 (A, D), LC3 (B, E), and the merged images (C, F). Scale bar = 7 μm. (**G**) The numbers of LC3-immunoreactive autophagic figures per neuron determined in $Cdnf^{+/+}$ (green) and $Cdnf^{-/-}$ (magenta) mice are compared. Background level of green fluorescent puncta is also illustrated (white). Autophagy is significantly greater in $Cdnf^{-/-}$ than in $Cdnf^{+/+}$ mice; Two-tailed t-test (with Welch's correction) $t = 6.062$ df = 17.07. (H) Density of autophagosomes was determined in electron micrographs of submucosal and myenteric neurons of the ileum of $Cdnf^{+/+}$ ($n = 4$) and $Cdnf^{-/-}$ ($n = 4$) mice. Autophagic figures are more abundant in the submucosal neurons of $Cdnf^{-/-}$ than of $Cdnf^{+/+}$ animals; two-tailed t-test (with Welch's correction) $t = 3.761$ df = 87.16). This difference between genotypes is not apparent in the myenteric plexus ($p = .9289$, $t = 0.08955$ df = 82.89). (I) Density of autophagosomes was determined in electron micrographs of submucosal and myenteric neurons of the colon of $Cdnf^{+/+}$ ($n = 4$) and $Cdnf^{-/-}$ ($n = 4$) mice. Autophagic figures in $Cdnf^{-/-}$ mice are more abundant than in $Cdnf^{+/+}$

animals, both in the submucosal (two-tailed t-test $t = 3.326$, df = 43.49) and myenteric neurons (two-tailed t-test $t = 2.296$ df = 84.97). (J-M). Transmission electron microscopic images of autophagosomes (arrows) in submucosal neurons of $Cdnf^{+/+}$ ileum (J), $Cdnf^{-/-}$ ileum (K), $Cdnf^{+/+}$ colon (L), and $Cdnf^{-/-}$ colon (M). Scale bars = 500 nm.
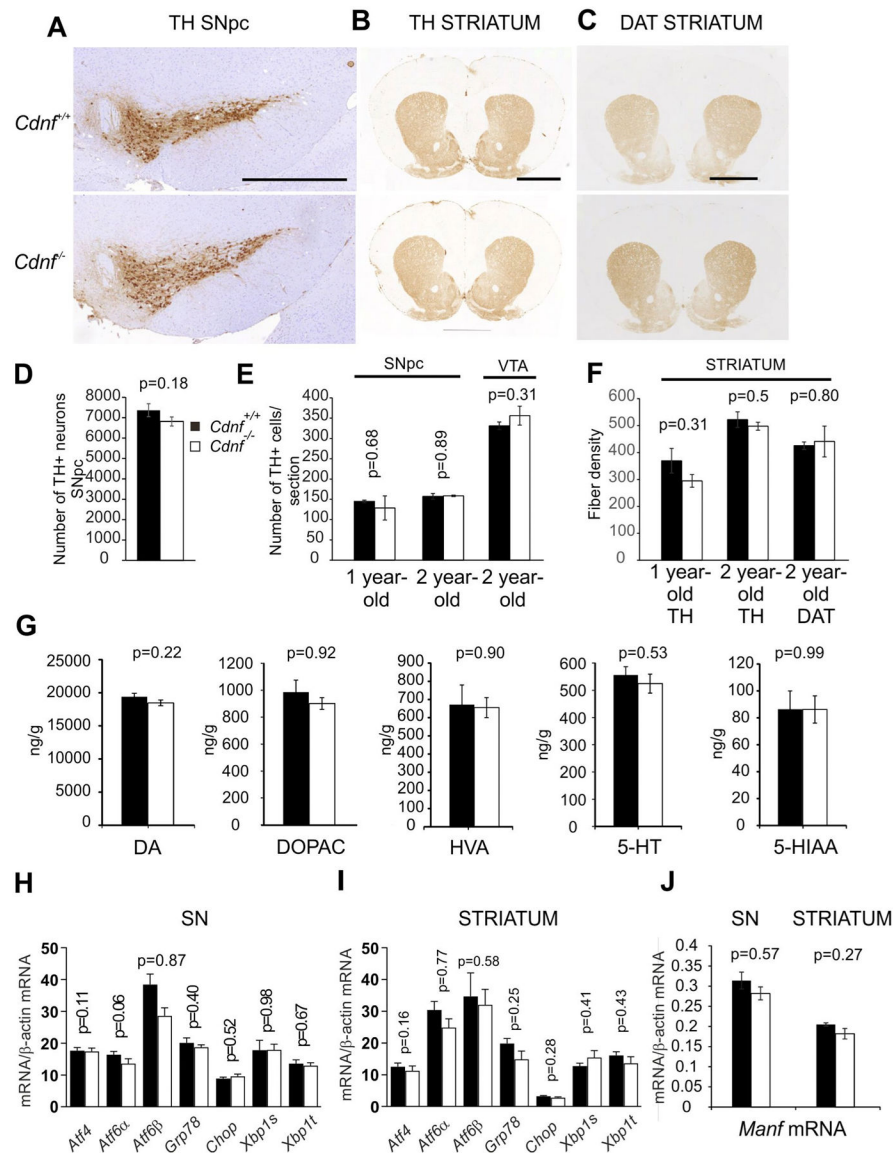
Fig. 6. Characterization of midbrain dopamine system in *Cdnf*$^{-/-}$ and *Cdnf*$^{+/+}$ mice.
(**A-C**) Representative pictures of coronal sections from 2 year-old *Cdnf*$^{+/+}$ (upper panel) and *Cdnf*$^{-/-}$ (lower panel) mouse brains immunostained with antibodies to TH and DAT at the level of the substantia nigra pars compacta (SNpc) and striatum. Scale bars: **A** = 100 μm, **B-C** = 200 μm. (**D**) Number of TH-positive neurons was quantified in the SNpc from *Cdnf*$^{+/+}$ (*n* = 4) and *Cdnf*$^{-/-}$ (*n* = 7) 12 month-old male mice. (**E**) No differences were found between genotypes in the proportion of dopaminergic neurons quantified from scanned slides of TH-stained sections of SNpc of 9–12 month-old male mice (*n* = 2–3 mice/genotype) and SNpc and VTA from 2 year-old male mice (*n* = 3–4 mice/genotype) (**F**). TH-positive striatal fiber densities did not differ between *Cdnf*$^{+/+}$ and *Cdnf*$^{-/-}$ mice quantified from 1 year-old mice (*n* = 2–3). No differences were found in striatal TH- and DAT-immunoreactive fiber densities in 2 year-old *Cdnf*$^{+/+}$ and *Cdnf*$^{-/-}$ mice (*n* = 3–4) mice. (**G**) Dopamine (DA), DOPAC, HVA, serotonin (5-HT) and 5-HIAA concentrations were

similar in striata from *Cdnf*^{+/+} and *Cdnf*^{-/-} mice measured by HPLC from 9 to 12 month-old male mice (*Cdnf*^{+/+} mice $n = 10$, *Cdnf*^{-/-} mice, $n = 11$, t-test; for DA and DOPAC, Mann Whitney U test). (**H–I**) qPCR analysis of transcripts encoding UPR-markers in SN (**H**) and striatum (**I**) of 9–12 month-old *Cdnf*^{+/+} ($n = 3$) and *Cdnf*^{-/-} ($n = 5$) male mice. (**J**) qPCR analysis of transcripts encoding *Manf* in the SN and striatum of 9–12 months *Cdnf*^{+/+} ($n = 6$) and *Cdnf*^{-/-} ($n = 6$) mice. Mean ± SEM, *$p < .05$.
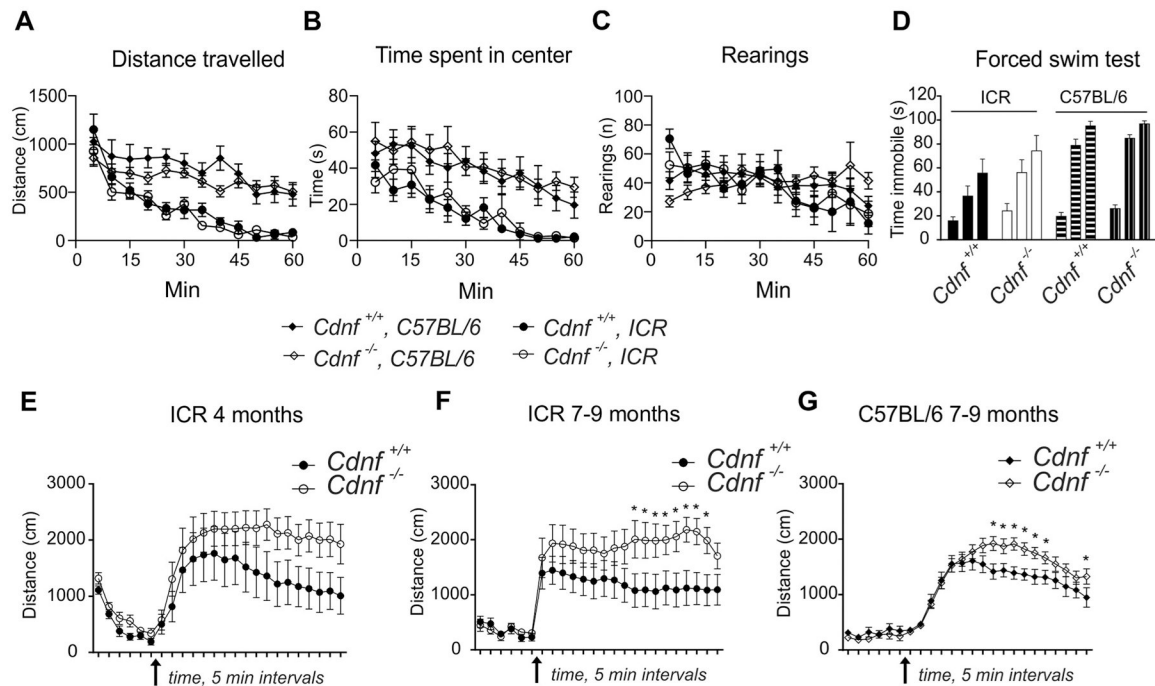
Fig. 7. Age-dependent increase in amphetamine-induced activity.
Novelty-induced locomotor activity measured in 7 month-old mice on mixed or C57BL/6 backgrounds. (**A**) Distance travelled; mixed ICR background the effect of genotype $F(1,19) = 0.8$, $p = .38$, interaction of genotype and time $F(11,209) = 1.4$, $p = .19$; C57BL/6 background effect of genotype $F(1,24) = 1.2$, $p = .28$, interaction of genotype and time $F(11,264) = 7.6$, $p = .12$; (**B**) time spent in the center; mixed ICR background the effect of genotype $F(1,19) = 0.1$, $p = .74$, interaction of genotype and time $F(11,209) = 0.7$, $p = .78$; C57BL/6 background effect of genotype $F(1,24) = 0.2$, $p = .63$, interaction of genotype and time $F(11,264) = 0.4$, $p = .96$; (**C**) vertical activity, measured for one hour; mixed background the effect of genotype $F(1,19) < 0.001$, $p = .99$, interaction of genotype and time $F(11,209) = 0.8$, $p = .65$; C57BL/6 background effect of genotype $F(1,24) = 0.008$, $p = .93$, interaction of genotype and time $F(11,264) = 2.0$, $p = .03$; (**D**) Forced swim test in water-filled cylinder measuring immobility time in for six minutes in two-minute intervals; mixed background, effect of genotype $F(1,19) = 1.6$, $p = .22$, interaction of genotype and time $F(2,38) = 0.8$, $p = .46$; C57BL/6 background, effect of genotype $F(1,24) = 1.5$, $p = .23$, genotype by time interaction $F(2,48) = 0.5$, $p = .63$ (2-way RM ANOVA). For A-D, male mice used, $n = 10–14$). Amphetamine-induced (3 mg/kg) activity was recorded for 90 min (after 30 min habituation in open field) for 4 month-old male mice in mixed ICR genetic background (**E**), $n = 10$; 2-way RM ANOVA the effect of genotype $F(1,18) = 2.0$, $p = .176$; time $F(17,306) = 12.7$, $p < .0001$; interaction of genotype and time $F(17,306) = 1.8$, $p = .026$; and for 7–9 month-old on mixed background (**F**), $n = 10–11$, 2-way RM ANOVA the effect of genotype $F(1,19) = 3.3$, $p = .086$; time $F(17,323) = 0.7$, $p = .840$; interaction of genotype and time $F(17,323) = 2.0$, $p = .010$; and C57BL/6 background (**G**), $n = 12–14$, 2-way RM ANOVA the effect of genotype $F(1,24) = 2.9$, $p = .102$; time $F(17,408) = 59.1$, $p < .0001$; interaction of genotype and time $F(17,408) = 3.8$, $p < .0001$.
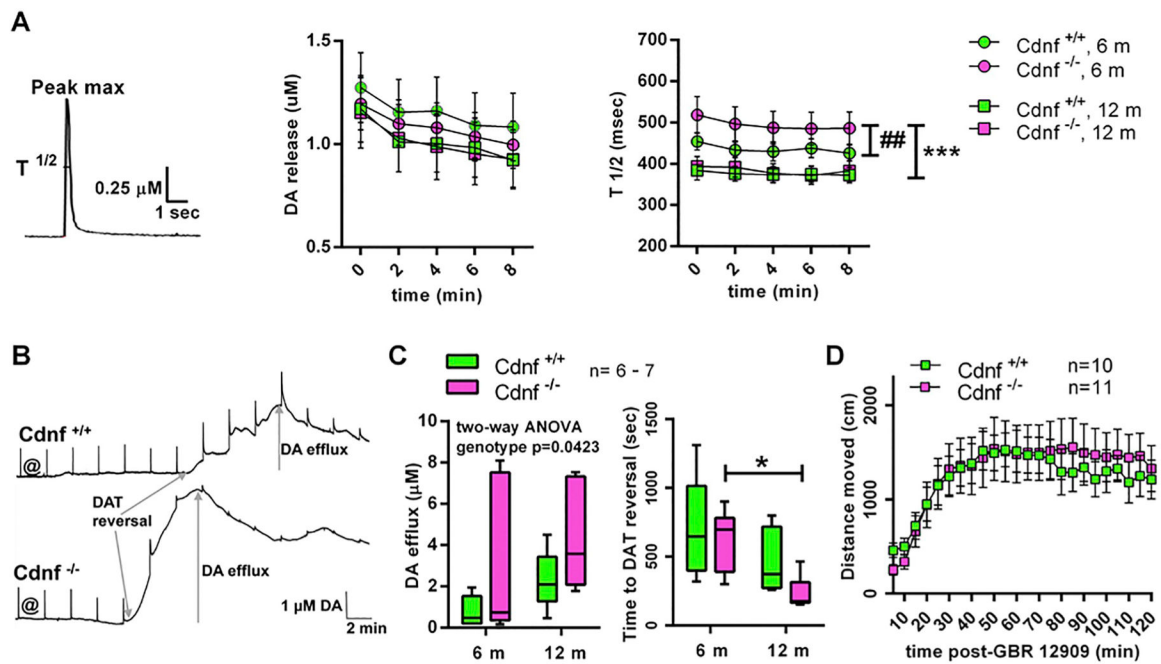
Fig. 8. Age-dependent changes in the function of DA neurons in *Cdnf*^{-/-} mice.
(**A**) Striatal slices were stimulated electrically every two minutes to evoke DA release (see the representative DA trace). The levels of the DA released (Peak max) were similar in *Cdnf*^{+/+} and *Cdnf*^{-/-} mice (F (3, 50) = 0.2092, *P* = .8896, 2 way RM ANOVA). The half-widths of the events (T½) were longer in 6 month-old *Cdnf*^{-/-} mice suggesting that they had slower reuptake of DA than the *Cdnf*^{+/+} mice at this age, but no differences between the genotypes could be found in the 12 month-old mice anymore (genotype: F(3, 50) = 18.04, p < .0001, 2 way RM ANOVA, ## between adult *Cdnf*^{+/+} and *Cdnf*^{-/-}, *p* = .007, *** between 6 month-old and 12 month-old *Cdnf*^{-/-}, *p* < .0001, Tukey's). (**B**) Representative traces from the recordings with amphetamine perfused over the striatal slices of *Cdnf*^{+/+} and *Cdnf*^{-/-} mice. Electrically stimulated dopamine transients were evoked at 2 min intervals. Amphetamine was added to perfusion at @. The reversal of the direction of DAT transport can be seen as a start of a large slow shift in the baseline representing the DA efflux. (**C**) The amphetamine-induced DAT-mediated DA efflux was higher in *Cdnf*^{-/-} mice than in *Cdnf*^{+/+} animals, a difference that was more pronounced in the 12 month-old animals (F(1,21) = 4.673, *p* = .0423, 2 way ANOVA). DAT reversal occurred at an earlier time point in 12 month-old *Cdnf*^{-/-} mice than in 6 month-old *Cdnf*^{-/-} mice (age: F(1,21) = 10.42, *p* = .004, two-way ANOVA, * *p* = .0468, Tukey's). (**D**) Locomotor activity in an open field arena after GBR 12909 injection (1 year-old mice) was similar in both genotypes (F(1,19) =0.04056, *p* = .8425, 2 way RM ANOVA).

Table 1

Apoptosis of neurons in the myenteric and submucosal plexuses of the ileum and colon of juvenile $Cdnf^{+/+}$ and $Cdnf^{-/-}$ mice.

Plexus	Region	Genotype	N (number mice/total neurons examined)	Apoptotic neurons (% total)
Myenteric	Ileum	$Cdnf^{+/+}$	4/22,301	0
Myenteric	Ileum	$Cdnf^{-/-}$	5/27,733	0.02 ± 0.02
Myenteric	Colon	$Cdnf^{+/+}$	4/28,819	0
Myenteric	Colon	$Cdnf^{-/-}$	6/44,603	0.01 ± 0.01
Submucosal	Ileum	$Cdnf^{+/+}$	4/4989	0.02 ± 0.02
Submucosal	Ileum	$Cdnf^{-/-}$	5/4740	0.09 ± 0.03
Submucosal	Colon	$Cdnf^{+/+}$	4/1784	0.07 ± 0.07
Submucosal	Colon	$Cdnf^{-/-}$	6/1452	0.12 ± 0.08